Sumoylation of RNA Polymerase II Regulates Transcription in *Saccharomyces cerevisiae*

Benjamin G. Bergey

A thesis submitted to the Faculty of Graduate Studies in Partial Fulfillment of the Requirements for the Degree of Master of Science

Graduate Program in Biology
York University
Toronto, Ontario
May 2024

Abstract

Sumoylation is a post-translational modification that is involved in a host of cellular processes, including important roles in transcription. While it was previously reported that Rpb1, the largest subunit of RNA polymerase II (RNAPII), is sumoylated following UV-stress, our lab has shown that Rpb1 is also sumoylated under normal growth conditions. Here, we show that sumoylated Rpb1 is mostly associated with chromatin, providing further support for its role in transcriptional processes. We also show that the SUMO protease Ulp2 is important for supporting basal sumoylation of Rpb1, rather than merely as an instrument for desumoylation, which is an unexpected finding. Moreover, while impairing Rpb1 sumoylation at its major sumoylation site, K1487, has no apparent effect on growth, nascent transcription analysis from Global Run-on Sequencing (GROseq) reveals that a small number of genes are upregulated in this sumoylation-deficient Rpb1 mutant, a quarter of which are involved in the stress response.

Acknowledgements

I have many people to thank for making this research project such a positive experience. I want to first thank Su and Marjan for everything that makes great long-standing lab members: being open to discussing lab work and projects; expressing sympathy for unexpected results (not the good kind); and just genuinely being kind and thoughtful people who make coming to the lab an enjoyable thing to do. Former members of the Rosonina lab: Mohammad, Veroni, Giovanni, Yimo, Nujhat, Mostafa, Anthea, Fadi, Verne, Mahtab, Anna, Jessica, Josh, Atara, John, and Akhi, I am grateful to all of you for creating a welcoming and fun research environment over the years.

Thank you also to Dr. Peter Cheung for your guidance throughout this project as a member of my supervisory committee, and to Dr. Mark Bayfield and Dr. Bill Kim for taking the time and effort to be on my examining committee.

I want to thank Dr. Emanuel Rosonina for quite a lot. Thank you for encouraging me in my aspirations to enroll as a graduate student and for supporting me throughout my research. Despite the winding nature of my project and the frustrations I often felt, I left each of our meetings with a clearer head and stronger sense of direction than when I first sat down. Your ability to see my experimental problems more frequently as hiccups rather than roadblocks helped instill a confidence that left me energized to tackle the next step. Your mentorship has been invaluable to me as a researcher and a scientific professional, and I am sincerely grateful for that.

Most importantly, thank you to my wife and family for believing in me and for suffering my long hours (sometimes) and even longer sighs. May you never read this. And thank you Bryan, for everything.

Table of Contents

List of Tables

List of Figures

List of Abbreviations

°C	Degrees Celsius
AEBSF	4-(2-aminoethyl)benzenesulfonyl fluoride hydrochloride
Anti-BrdU	bromodeoxyuridine-binding antibody
ATP	Adenosine triphosphate
Br-UTP	Bromouridine-triphosphate
cDNA	Complementary deoxyribonucleic acid
ChIP	Chromatin immunoprecipitation
Chrom.	Chromatin bound fraction
ChrV	Chromosome V
CPM	Counts per million
CTD	Carboxy-terminal domain
C-terminal	Carboxy-terminal
CTP	Cytidine triphosphate
ddH2O	Double distilled water
DEPC	Diethyl pyrocarbonate
dH2O	Distilled water
DNA	Deoxyribonucleic acid
dNTP	Deoxyribonucleotide triphosphate
DTT	Dithiothreitol
EDTA	Ethylenediaminetetraacetic Acid
ESR	Environmental stress response
FDR	False discovery rate
Fig	Figure
g	Gram
g (italic)	*g*-force
GO	Gene Ontology
GROseq	Global Run-on Sequencing
GTF	General transcription factor
GTP	Guanosine triphosphate

HA	Human influenza hemagglutinin
HCl	Hydrochloric acid
HEPES	4-(2-hydroxyethyl)-1-piperazineethanesulfonic acid
HRP	Horseradish peroxidase
HTS	High-throughput sequencing
IB	Immunoblot
IgG	Immunoglobulin G
IGV	Integrative Genomics Viewer
IP	Immunoprecipitation
J	Joule
KCl	Potassium chloride
kDa	Kilodalton
KlTRP1	*Kluyveromyces lactis* TRP1 marker gene
KOAc	Potassium acetate
KOH	Potassium hydroxide
LiAc	Lithium acetate
Lys/K	Lysine
M	Molar
MDS	Multidimensional scaling
MgOAc	Magnesium acetate
min	Minute
mL	Millilitre(s)
mM	Millimolar(s)
mRNA	Messenger ribonucleic acid
NaCl	Sodium chloride
NaOAC	Sodium acetate
NaOH	Sodium hydroxide
NEM	N-ethylmaleimide
NGS	Next-generation sequencing
NP40	Nonylphenoxypolyethoxylethanol
N-terminal	Amino-terminal

OD	Optical density
ORF	Open reading frame
PBS	Phosphate buffer saline
PBST	Phosphate buffer saline with Tween
PCR	Polymerase chain reaction
PEG	Polyethylene glycol
PIC	Preinitiation complex
PIPES	Piperazine-N,N′-bis(2-ethanesulfonic acid)
PMSF	Phenylmethylsulfonyl fluoride
PTM	Post-translational modification
qPCR	Quantitative polymerase chain reaction
R	Argenine
RNA	Ribonucleic acid
RNAPI	RNA polymerase I
RNAPII	RNA polymerase II
Rpb1	RNA polymerase II subunit 1
Rpb3	RNA polymerase II subunit 3
RPG	Ribosomal protein gene
rRNA	Ribosomal ribonucleic acid
RT	Room temperature
RT-qPCR	Real-time quantitative polymerase chain reaction
s	Second(s)
S. cerevisiae	*Saccharomyces cerevisiae*
SC	Synthetic Complete
SDS-PAGE	Sodium dodecyl sulfate - polyacrylamide gel electrophoresis
SEM	Standard error of the mean
Seq	Sequencing
Soluble	Soluble fraction
SS-carrier DNA	Salmon sperm-carrier deoxyribonucleic acid
SSPE	Saline-sodium phosphate-EDTA
STUbL	SUMO-Targeted Ubiquitin Ligase

SUMO	Small ubiquitin-like modifier
TBP	TATA-binding protein
TCA	Trichloroacetic acid
TF	Transcription factor
Tfg1	Transcription initiation factor IIF subunit alpha
TFIIF	Transcription factor II F
Tris	Trisaminomethane
tRNA	Transfer ribonucleic acid
TSS	Transcription start site
U	Unit
ug	Microgram
uL	Microlitre
uM	Micromolar
UV	Ultraviolet
WB	Western blot
WCE	Whole cell extract
YPD	Yeast extract peptone dextrose
yPIC	Yeast protease inhibitor cocktail

Section 1: Introduction

1.1 Sumoylation

Most post-translational modifications (PTMs) involve the attachment of small functional groups or proteins to a given target to alter its functionality or to allow it to perform a wider variety of tasks and to be regulated for the appropriate cellular context (Alquezar et al., 2021). Small ubiquitin-like modifiers (SUMO) are part of the large family of ubiquitin modifiers and have been studied extensively since their discovery almost 30 years ago. Sumoylation has since been reported to be involved in an ever-increasing scope of biological processes (Vertegaal, 2022). Identified originally as a modification of RanGAP1 to facilitate binding to the nuclear pore complex (Matunis et al., 1998), sumoylation has since been linked to everything from cell differentiation, stress response, cancer, and the burgeoning domain of condensate formation (Vertegaal, 2022).

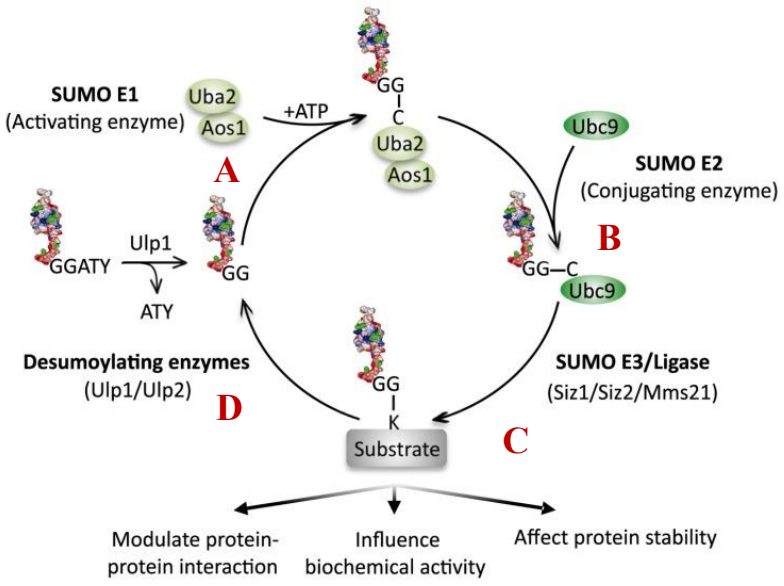

Figure 1: The sumoylation cycle. A) An immature SUMO is cleaved by Ulp1 to reveal a di-glycine that attaches to the E1 activating heterodimer Uba2/Aos1 then bonds with the mature SUMO in an ATP-dependent reaction. **B)** The SUMO-Uba2/Aos1 complex is transferred to the E2 conjugating enzyme, Ubc9, which targets and transfers the SUMO modifier to the substrate. **C)** SUMO is conjugated to the target substrate, often with the assistance of an E3 ligase. **D)** Deconjugating enzymes Ulp1 and Ulp2 cleave SUMO from the target substrate (Ulp1) or reduce SUMO chains (Ulp2). (Adapted from Cremona et al., 2012).

The process of sumoylation is similar to that of ubiquitination, involving several conjugation and deconjugation enzymes (Figure 1). In *S. cerevisiae*, the cycle begins with a precursor form of SUMO being cleaved at its C-terminal end by the SUMO protease Ulp1 to reveal a di-glycine motif which becomes the functional region that attaches to an exposed lysine on target substrates (Cremona et al., 2012; Pabst et al., 2019). The E1 activating heterodimer Uba2/Aos1 then bonds with the C-terminal end of the mature SUMO in an ATP-dependent reaction and transfers it to a cysteine residue of the E2 conjugating enzyme, Ubc9. The Ubc9-SUMO complex subsequently targets and transfers the SUMO modifier to the substrate, forming an isopeptide bond between the C-terminal domain of SUMO and a side-chain lysine residue on the target substrate. Conjugation to the substrate is often accomplished with the help of an E3 ligase that tends to be context-specific, and of which several have been identified in *S. cerevisiae*, including Siz1, Siz2, Mms21 (Cremona et al., 2012; Pabst et al., 2019) and others.

This process is a reversible one, by way of the two ubiquitin-like proteases in *S. cerevisiae*: Ulp1 and Ulp2 (Eckhoff & Dohmen, 2015; Hickey et al., 2012; Pabst et al., 2019). The cysteine-protease function of Ulp1 (which exposes the di-glycine motif of the immature SUMO) enables it to target sumoylated proteins for cleavage from the conjugate (Hickey et al., 2012; Bylebyl et al., 2003). Like ubiquitin, once a substrate has been SUMO-modified, additional SUMOs can attach to the conjugated SUMO to form a chain (termed "polysumoylation") of accumulated SUMO moieties (Tatham et al., 2001). Ulp1 is a cysteine protease that acts in a stochastic manner, cleaving both SUMO-substrate bonds as well as SUMO chain links with equal efficiency (i.e. SUMO-SUMO bonds) (Hickey et al., 2012; Eckhoff & Dohmen, 2015). Though Ulp1 is capable of cleaving SUMO-SUMO bonds, Ulp2 is the primary SUMO protease responsible for reducing accumulated SUMO chains on polysumoylated

substrates (Hickey et al., 2012; Eckhoff & Dohmen, 2015; Bylebyl et al., 2003). This is achieved in "exo" fashion, where SUMO groups are sequentially removed beginning from the most distal SUMO group in the chain, and working inwards (Eckhoff & Dohmen, 2015).

While deletion of *ULP1* is lethal, deletion of *ULP2* is tolerated in yeast, but with damaging effects. *ulp2Δ* mutants exhibit poor growth, heat sensitivity, and, among other negative phenotypes, susceptibility to aneuploidy in order to manage the significant stress levelled by loss of this SUMO protease (Ryu et al., 2016; Bylebyl et al., 2003). Loss of Ulp2 has also been shown to decrease the association of RNAPII with chromatin at actively transcribed genes resulting in downregulated gene expression (Ryu et al., 2019).

1.2 RNA Polymerase II (RNAPII) and sumoylation of Rpb1

RNA transcription is an essential biological process that transmits the genetic information encoded in DNA into its functional counterpart, RNA. In eukaryotes, three types of RNA polymerase carry out transcription: RNA Polymerase I (RNAPI) transcribes ribosomal RNA (rRNA), RNA Polymerase II (RNAPII) transcribes all protein-coding genes, and RNA Polymerase III (RNAPIII) transcribes tRNAs, 5S rRNA, and, along with RNAPII, small nuclear RNAs (Cramer et al., 2008; Watson et al., 2004). RNAPII is the most studied of these, as it transcribes all mRNAs and is subject to extensive regulation (Muniz et al., 2021). Transcription proceeds in three general phases: Initiation, where, along with a set of general transcription factors (GTFs), RNAPII is recruited to gene promoters to form a pre-initiation complex (PIC) and synthesizes the initial bases of RNA; Elongation, where RNAPII is stimulated by several new factors that release it from the PIC and begins processing tasks such as 5' capping and splicing, and; Termination, where the polymerase dissociates from DNA and a mature mRNA is released (Watson et al., 2004; Osman & Cramer, 2020).

Rpb1 is the largest subunit of RNAPII and it plays a crucial role in regulating transcription. In addition to harbouring the active site of RNA synthesis, Rpb1 contains a unique unstructured C-terminal domain (CTD) that consists of 26-repeats (in *S. cerevisiae*) of the heptapeptide sequence Tyr1-Ser2-Pro3-Thr4-Ser5-Pro6-Ser7 (Suh et al., 2013) which undergoes extensive post-translational modifications (PTMs) during transcription (Harlen & Churchman, 2017). One of the most well-characterized of these modifications is phosphorylation, which reliably signals RNAPII's transcriptional stage. For instance, newly recruited RNAPII has an unphosphorylated CTD, Ser5-phosphorylated CTD is associated with RNAPII at the PIC, and Ser2-phosphorylated CTD is associated with elongating RNAPII (Harlen & Churchman, 2017).

The CTD is attached to the body of Rpb1 by a flexible linker region which has recently been shown to facilitate the proper functioning of elongating RNAPII. The cyclin-dependent kinase Bur1 phosphorylates several residues within the linker that subsequently recruit Spt6 (Chun et al., 2019), a transcriptional activator that has been shown to stimulate RNAPII-elongation, assist with mRNA processing, and help reassemble nucleosomes behind the extending polymerase (Vos et al., 2018; Sdano et al., 2017). That Spt6 binds to the Rpb1 linker is relevant for this project because it is also a site of significant Rpb1-sumoylation (Figure 2), the impact of which is explored in this work.

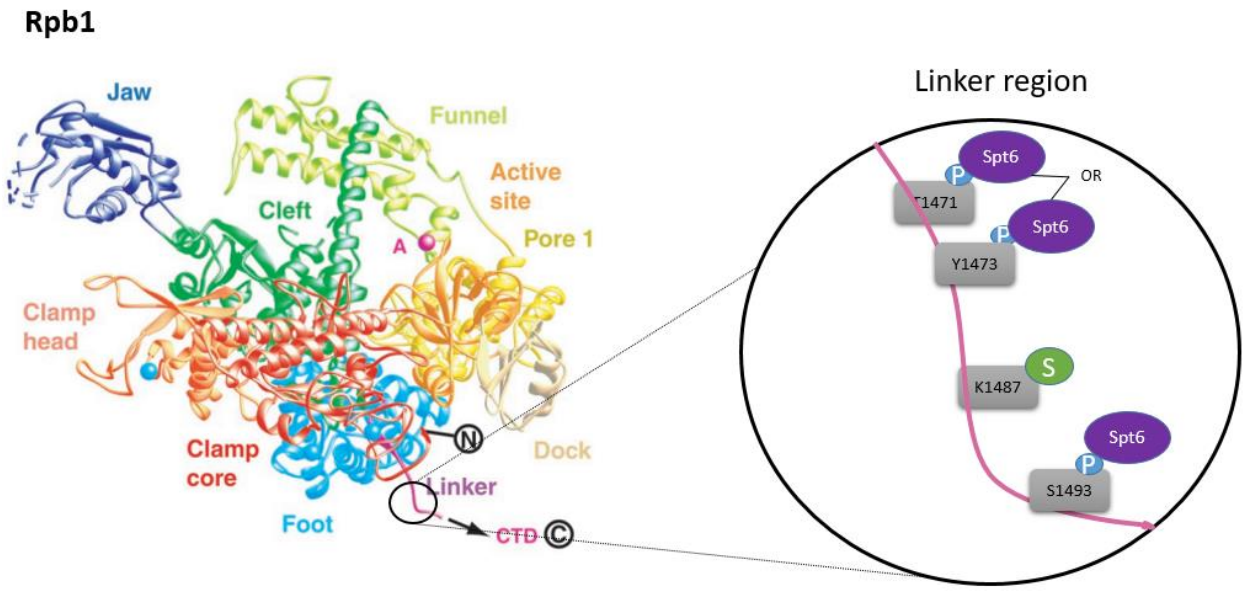

Figure 2: **PTMs at the Rpb1 linker region.** Rpb1 is sumoylated in the Rpb1 linker region at K1487 (green dot). Spt6 has been reported to bind phosphorylated residues (blue dots) just upstream (T1471 or Y1473) and downstream (S1483) of K1487R. (Adapted from Cramer et al., 2001).

Rpb1 sumoylation was first detected in response to UV-stress, and the major sumoylation site was identified in the linker region, at Lys-1487 (Chen et al, 2009). In its investigation of the function of sumoylated Rpb1, this study reported little cellular impact of a SUMO-impaired Rpb1, concluding that Rpb1 sumoylation was primarily involved in restraining the DNA damage checkpoint response. But subsequent research showed that Rpb1 sumoylation also supported UV-induced degradation of elongating Rpb1, and suggested this may enable repair mechanisms to better access DNA lesions blocked by the stalled polymerase (Heckmann et al., 2019). While the published research to date characterizes sumoylated-Rpb1 as merely a UV-induced phenomenon, recent work in our lab found that Rpb1 sumoylation can be detected under normal growth conditions (Travas, 2021). This is an especially intriguing finding, as it suggests that sumoylation may regulate transcriptional processes in ways that have been unexplored and that are not related to the stress response.

1.3 The role of sumoylation in transcription

Though sumoylation is a PTM involved in many diverse cellular processes, proteins involved in transcription constitute one of the largest groups of SUMO targets (Vertegaal, 2022). Proteomic studies have identified pre-mRNA splicing, chromatin remodeling and transcriptional regulation to be some of the most heavily represented clusters of sumoylated proteins that are associated with gene expression (Hendriks & Vertegaal, 2016). While early studies found that sumoylation of transcription-associated proteins largely functioned to repress transcriptional activity (Hay, 2006; Rosonina, 2019), recent studies have challenged that broad characterization (Figure 3). Rosonina (2010) reported that reduced global levels of SUMO conjugates was associated with reduced RNAPII occupancy at several constitutive gene promoters, and further work by Moallem et al. (2023) found transcriptional changes in about a quarter of all protein-coding genes when global levels of sumoylation were reduced, with roughly half being upregulated and half downregulated (Figure 3A).

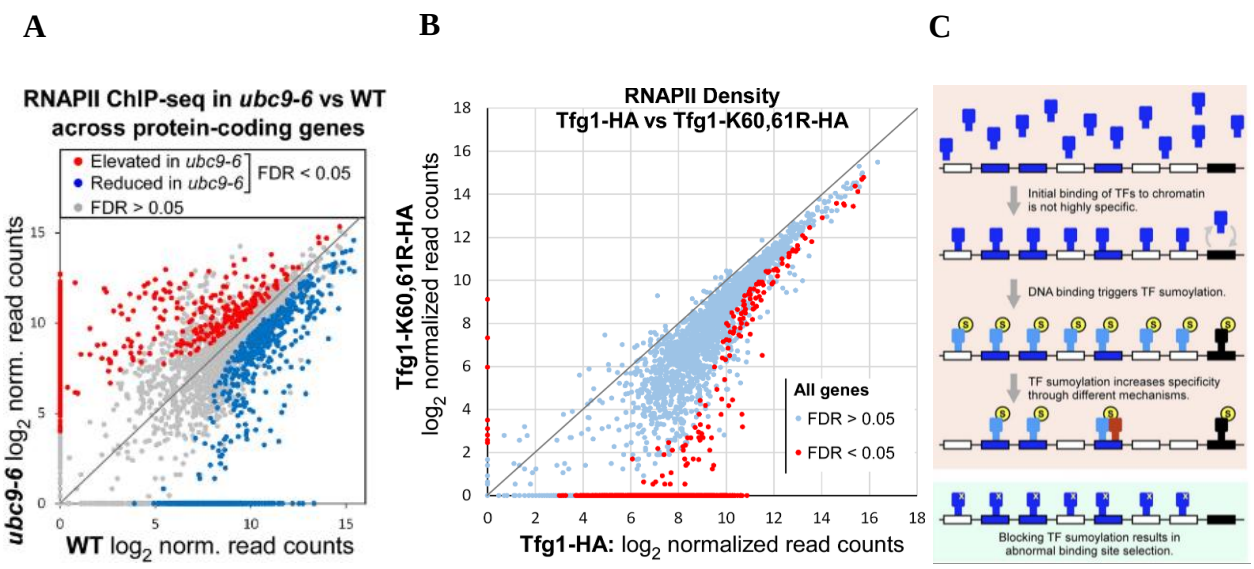

Figure 3: Impact of sumoylation on transcriptional processes. Scatterplots of differentially bound genes (RNAPII-ChIPseq) (**A** & **B**). **A)** Comparison of WT and *ubc9-6* (reduced global levels of sumoylation) strains. Roughly a quarter of all protein-coding genes are either upregulated or downregulated (sites with FDR < 0.05 shown with coloured dots: red indicates upregulated genes in the *ubc9-6* mutant, blue indicates downregulated genes in the *ubc9-6* mutant) (from Moallem et al., 2023). **B)** Comparison of Tfg1-HA and Tfg1-K60,61R-HA strains. The majority of differentially bound sites (sites with FDR < 0.05 shown with red dots) indicate widespread reduction in binding in the SUMO-deficient Tfg1 mutant (tfg1-K60,61R-HA) (from Baig et al., 2021). **C)** Proposed model of SUMO-dependent TF-binding specificity. Once bound to DNA, TF-sumoylation increases binding specificity such that only appropriate sites remain bound (from Rosonina, 2019).

Turning specifically to transcription factors (TFs), research examining how TF-sumoylation impacts TF-DNA binding and associated transcriptional effects reveals a complicated landscape. Chymchowitch et al. (2015) found that SUMO targeted the Rap1 transcription factor to positively regulate transcription at ribosomal protein genes (RPGs), and Baig et al. (2021) reported that impaired sumoylation of Tfg1, the largest subunit of TFIIF and most sumoylated general transcription factor (GTF), caused a widespread reduction in transcription (Figure 3B). Interestingly, however, constitutive sumoylation of this subunit also appears to generally curb transcription, as well as reducing its association with RNAPII (Baig et al., 2021). In a 2019 review, Rosonina proposed a model whereby some sequence-specific TFs become sumoylated after they bind DNA, facilitating their subsequent dissociation and

ultimately controlling their binding specificity (Rosonina, 2019). Importantly, however, this review highlights the fact that the resulting transcriptional effects are often nuanced and context-dependent, emphasizing that a general rule or mechanism for SUMO-dependent transcription remains unclear (Rosonina, 2019).

Despite the complexity implied from these findings, it is nevertheless encouraging that Rpb1 sumoylation has been detected in our lab under normal growth conditions. As RNAPII is the fundamental component that underpins mRNA transcription, characterization of its sumoylated form may uncover broader insights into the role of SUMO in transcriptional processes. My hypothesis is that Rpb1 sumoylation has a function during normal growth conditions to regulate transcription. My objectives in this thesis are thus to characterize and explore the function of Rpb1 sumoylation under normal (non-stressed) growth. Accordingly, I conduct several characterization studies of sumoylated Rpb1. Remarkably, I show that a significant fraction of chromatin-associated Rpb1 is sumoylated, implying its important role in transcriptional processes. I also show that a sumoylation-impaired Rpb1 is associated with an increase in nascent transcription for roughly two dozen genes, more than a quarter of which are associated with the stress response. Interestingly, further characterizations reveal that a sumoylation-impaired Rpb1 does not appear to impact normal growth, steady state RNA levels, or the association of Rpb1 with the transcriptional activator Spt6.

Section 2: Materials and Methods

2.1 Immunoprecipitation of Fractionated Chromatin

30 mL of W303a cells were grown to log phase in YPD, harvested by spinning at 3000 *g* for 5 min, resuspended in 6.25 mL Resuspension Buffer 1 (0.1 M PIPES/KOH, pH 9.4; 0.01 M DTT) and incubated at 30°C for 10 min with shaking. Cells were then spun, decanted and resuspended in 2.5 mL Buffer 2 (0.6 M sorbitol; 0.025 M Tris, pH 7.5; 67.5% YPD) with 500 U zymolyase and incubated at 30°C for 25 min with shaking. Cells were then spun for 3 min at 850 *g*, decanted, and resuspended in 2.5 mL Buffer 3 (0.7M sorbitol; 0.025 M Tris, pH 7.5; 62.5% YPD) and incubated at 30°C for 20 min with shaking. Cells were then spun at 850 *g* for 3 min, decanted, and washed 3X with 1 mL Lysis Buffer (0.4 M sorbitol; 0.15 M KOAc, pH 7; 0.002 M MgOAc; 0.02 M PIPES/KOH, pH 6.8; 1 mM PMSF, 2.5 mg/mL NEM; 1 mM PMSF; 0.05 mM AEBSF; 0.7 uM E-64; 1.1 uM pepstatin; 250uM 1,10 Phenanthroline). Cells were then resuspended in 600 uL Lysis Buffer + 1% Triton X-100, mixed gently, and left on ice for 5 min with periodic gentle mixing. Sample was spun for 15 min at 20,000 *g* at 4°C, supernatant moved to another tube and spun once more to remove all cell debris (soluble). Pelleted fraction (chromatin) was washed 1X with Lysis Buffer and resuspended in Modified Sample Buffer (0.14 M Tris pH 6.8; 4% SDS). Chromatin and soluble fractions were then boiled for 5 min at 95°C, mixed well, and spun for 10 min at 20,000 *g* for 10 min at 4°C. Samples were topped up to 2 mL IP+ Buffer (50 mM Tris-HCl, pH 8; 150 mM NaCl; 1 mM EDTA, pH 8; 0.1% NP-40; 1 mM PMSF; 0.1 mM DTT; 2.5 mg/mL NEM; 0.05 mM AEBSF; 0.7 uM E-64; 1.1 uM pepstatin; 250 uM 1,10 Phenanthroline), 25 uL was removed for input (to which 25 uL 2X Sample Buffer was added, boiled for 5 min at 95°C and frozen at -20°C until ready to blot) and the remainder incubated with 15 uL Protein G-linked agarose beads and 1.2 ug of the 8WG16 antibody on a

rotator for 2 h at 4°C. IP'd material was pelleted by spinning beads for 1 min at 500 *g*. Washed 3X with IP Wash Buffer (50 mM Tris-HCl, pH 8; 150 mM NaCl; 1 mM EDTA, pH 8; 1% NP-40; 1 mM PMSF) and 2X with IP Buffer (50 mM Tris-HCl, pH 8; 150 mM NaCl; 1 mM EDTA, pH 8), resuspended in 100uL 2X Sample Buffer (140 mM Tris-HCl, pH 6.8; 4% SDS; 20% glycerol; 0.02% bromophenol blue) and heated at 95°C for 5 min then stored at -20°C.

2.2 Immunoprecipitation

10-20 mL of cells were grown to exponential phase, harvested by spinning at 3000 *g* for 5 min to remove media, then washed once with ice cold IP+ Buffer (50 mM Tris-HCl, pH 8; 150 mM NaCl; 1 mM EDTA, pH 8; 0.1% NP-40; 1 mM PMSF; 0.1 mM DTT; 2.5 mg/mL NEM; 0.05 mM AEBSF; 0.7 uM E-64; 1.1 uM pepstatin; 250 uM 1,10 Phenanthroline). 300 mg acid-washed glass beads and 0.5 mL IP+ Buffer were then added to washed cells and vortexed for 30 min (2 x 15 min with 5 min break on ice halfway through) at 3000 *g* at 4°C. Lysate was moved to a new tube, glass beads washed with IP+ Buffer and added to lysate in a total volume of ~1 mL. 25 uL was removed for input (to which 25 uL 2X Sample Buffer was added, boiled for 5 min at 95°C and frozen at -20°C until ready to blot) and remaining lysate incubated with 15 uL Protein G-linked agarose beads and 1.2 ug of the 8WG16 antibody on a rotator for 2 h at 4°C. IP'd material was pelleted by spinning beads for 1 min at 500 *g*. Washed 3X with IP Wash Buffer (50 mM Tris-HCl, pH 8; 150 mM NaCl; 1 mM EDTA, pH 8; 1% NP-40; 1 mM PMSF) and 2X with IP Buffer (50 mM Tris-HCl, pH 8; 150mM NaCl; 1mM EDTA, pH 8), resuspended in 100 uL 2X Sample Buffer (140 mM Tris-HCl, pH 6.8; 4% SDS; 20% Glycerol; 0.02% bromophenol blue) and heated at 95°C for 5 min and stored at -20°C.

2.3 Western Blot

Equal amounts of sample were resolved with SDS-PAGE gels of an appropriate percentage and transferred to nitrocellulose membranes. Membranes were washed for 30 min with Blocking Buffer (5% skim milk in PBST [0.05% Tween-20 in 1% PBS (Fisher Scientific)]) and incubated with primary antibodies according to experimental requirements (GAPDH, Rabbit, Sigma-Aldrich, 1:5000; H3, Rabbit, Abcam, 1:1000; SMT3, Santa Cruz, Rabbit 1:500; Rpb1, AB4224 (custom-made for E. Rosonina, targeting the N-terminal region of Rpb1), Rabbit, 1:1000; 8WG16, Santa Cruz, Mouse, 1:1000) overnight at 4°C. Membranes were subsequently washed 3X in PBST (5 min each), incubated with appropriate HRP-conjugated secondary antibodies (Thermofisher Scientific) at 1:5000 in PBST for 30 min at room temperature, washed again 3X in PBST (5 min each), and incubated with Clarity Western ECL Substrate solution (Bio Rad) for 5 min and exposed using MicroChemi chemiluminescence imager (DNR Bio Imaging).

2.4 Growth curve and Spot Assay

Samples were incubated overnight in 30°C incubator in YPD and grown to saturation. The following day, for growth curves, equal amounts of cells in media were added to fresh YPD in a 96-well plate at a starting OD of 0.1. Cultures were incubated at 30°C with shaking in the accuSkan FC (Thermo Fisher Scientific) automated spectrophotometer. Readings were taken every 15 min (blank-subtracted with YPD) for a total of 80 readings. Replicate OD_{595} were averaged for each strain at each time point to generate growth curve. For Spot Assays, the same overnight inoculum used for growth curves was used to add equal amounts of sample culture to YPD plates in serial 5X dilutions and incubated at 30°C. Spot assay plates were imaged following two days of growth.

2.5 UV treatment

Samples were grown to exponential phase in YPD (20 mL), centrifuged at 3000 *g* for 3 min and resuspended in an equal volume of PBS. Samples were transferred to 100 mm petri dishes, irradiated at 400 J, then transferred back to 50 mL tubes. Samples were then centrifuged at 3000 *g* for 3 min, supernatant removed and resuspended in 30 mL 30°C YPD. Samples were then covered in aluminium foil and transferred to a 30°C shaker for 20 min before centrifuging to prepare cells for immunoprecipitation (IP), as described in this section.

2.6 ChIP & ChIPseq

Samples were grown in synthetic complete (SC) medium to exponential phase (200 mL culture size), crosslinked with 1% Formaldehyde (37% (Thermofisher) first diluted to 11% in ChIP Diluent (143 mM NaCl; 1.43 mM EDTA; 70 mM HEPES-KOH, pH 7.5) then added to culture) for 20 min at room temperature with mixing every 5 min. Crosslinking was quenched with Glycine (300 mM final) for 5 min with occasional mixing, then split into 50 mL (4 x 50 mL for each sample) tubes and centrifuged for 5 min at 3000 *g*. Samples were washed twice with TBS (20 mM Tris-HCl, pH 7.5; 150 mM NaCl), resuspended in 1 mL of ChIP Lysis Buffer (50 mM HEPES-KOH, pH 7.5; 150 mM NaCl; 1 mM EDTA; 1% Triton X-100; 0.1% NaDeoxycholate; 0.1% SDS), centrifuged at 20,000 *g* for 5 min at 4°C and flash frozen in liquid nitrogen and stored at -80°C. (Only half the frozen sample (two tubes – the "sample group") was subsequently processed, and half saved for potential future study.) To the frozen samples, for each tube, 0.3 g of acid-washed glass beads and 600 uL of ChIP Lysis Buffer+ (ChIP Lysis Buffer plus 1 mM PMSF; 0.05 mM AEBSF; 0.7 uM E-64; 1.1uM pepstatin; 250 uM 1,10 Phenanthroline) was added, and cells were homogenized (Benchmark BeadBug) at max speed for 6 min total (two rounds of 6 x 30 second pulses, with 45 seconds between pulses and 2 min on ice between rounds). Separated lysate from glass beads and sonicated lysed material for a

total of 8 min (four rounds of 8 x 15 second pulses, with 15 seconds between pulses and 2 min on ice between rounds) in the Sonic Dismembrator Q700/FB-705 (Amplitude 40%). Centrifuged sonicated material for 5 min at 4°C at 20,000 *g* then incubated supernatant with 50 uL Protein G-conjugated magnetic beads (Dynabeads, Thermo Fisher Scientific) and 10 uL Anti-Rpb3 (Abcam) (per tube) overnight at 4°C on rotator. (Protein-G beads and Anti-Rpb3 were conjugated earlier in the day by incubating together for ~1 h at 4°C on a rotator in ChIP Lysis Buffer.) Samples were then washed once on a rotator at room temperature for 5 min with each of the following buffers: i) ChIP Lysis Buffer + NaCl (275 mM); ii) ChIP Lysis Buffer + NaCl (400 mM); ChIP Wash Buffer 3 (10 mM Tris-HCl, pH 8; 0.25 M LiCl; 1 mM EDTA; 0.5% NP-40; 0.5% NaDeoxycholate); TE (10 mM Tris-HCl, pH 8, 1 mM EDTA). Both tubes from each "sample group" were then merged by resuspending them together in 250 uL total of Elution Buffer (50 mM Tris-HCl, pH 7.5; 10 mM EDTA, pH 8; 1% SDS) and heated at 65°C for 20 min. Tubes were then placed against a magnet to separate ChIP material from magnetic beads and moved to a new tube. 250 uL TE was then added to beads, rotated at room temperature for 5 min, then added to ChIP material, now in a total volume of 500 uL. 10 uL of 10 mg/mL RNase A (EMD Millipore) was added to each sample and incubated for 1 h at 37°C. Samples were then incubated with 10 uL 20 mg/mL Proteinase K (BioShop) at 42°C for 1 h. Samples were then incubated overnight at 65°C to decrosslink ChIP material. DNA was then extracted using GeneJET Gel Extraction Kit (Thermo Fisher Scientific), and eluted in 40 uL TE, pH 8.0. ChIP-qPCR was then performed to determine relative RNAPII occupancy. (For qPCR, samples were diluted 10-fold to reserve sufficient material for high throughput sequencing.) To 5 uL of each sample, 1.5 uL 10 mM primer mix and 10.5 uL SYBR Green (FroggaBio SensiFAST SYBR No-ROX) were mixed, in duplicate, and loaded into a 96-well plate and placed in the qPCR machine

(Bio Rad CFX Opus 96) and run with the following settings: 95°C for 3 min, then 40 cycles of 95°C for 10 s / 60°C for 30 s. Signal was normalized to an untranscribed region of chromosome V (ChrV). To analyze RNAPII occupancy genome-wide, samples collected by ChIP were sent to SickKids Toronto for next-generation sequencing (NGS).

2.7 GROseq

Cultures were grown in synthetic complete (SC) medium to log phase (25 mL). Once harvesting OD was reached, an equal volume of ice was added to the cultures before being centrifuged at 1860 *g* for 5 min at 4°C, media removed and pellet resuspended in 10 mL of cold TMN buffer (10 mM Tris-HCl, pH 7.5; 5 mM $MgCl_2$; 100 mM NaCl) and placed on ice for 10 min. Samples were centrifuged again for 5 min at 4°C and resuspended in 1 mL DEPC-treated water + sarkosyl (0.6%) with gentle shaking for 25 min at 4°C to permeabilize. Samples were then centrifuged at 1200 *g* for 6 min at 4°C, supernatant removed, and pellet resuspended in 150 uL of Run-on Buffer (50 mM Tris-HCl, pH 7.5; 100 mM KCl; 10 mM $MgCl_2$; 2 mM DTT; 0.5 mM ATP; 0.5 mM CTP; 0.5 mM GTP; 0.5 mM Br-UTP) + 5 uL RNAse inhibitor (New England Biolabs) and incubated at 30°C for 5 min to complete the run on reaction. Sample was then topped up to 400 uL with AE buffer (50 mM sodium acetate, pH 5.2; 10 mM EDTA, pH 8.0, DEPC water) + SDS (0.9%) and mixed thoroughly. To extract RNA, an equal amount of phenol (pH 4.5) was added, mixed thoroughly, and subjected to two freeze/thaw cycles: 5 min in -80°C ethanol; 5 min in 65°C water bath, 1 min vortex in between cycles. Samples were frozen one more time in -80°C ethanol bath and centrifuged at 16,000 *g* for 7 min at room temperature. Aqueous layer was transferred to a new tube, to which 1.5X volumes of 1:1 phenol/chloroform was added, mixed, and centrifuged at 16,000 *g* for 5 min. The aqueous layer was again removed, to which 1.5X volumes of chloroform was added, mixed, and centrifuged at 16,000 *g* for 5 min.

RNA was precipitated by adding sodium acetate (0.1 M, pH 5.2) and 2.5X chilled 100% ethanol, left on ice for 15 min, and centrifuged at 20,000 *g* for 2 min at 4°C. Precipitated RNA was washed once with 70% ethanol, and, after the pellet dried sufficiently, resuspended in 100 uL DEPC-treated water. RNA was fragmented by adding NaOH (0.2 M), and incubated on ice for 20 min, then reaction was neutralized by adding 0.5 M Tris-HCl (pH 6.8). RNA was precipitated by adding an equal amount of isopropanol + 0.13 M NaOAC, inverted to mix, and precipitated for 15 min on ice. Samples were then centrifuged and washed with 70% ethanol, as described previously, pelleted, resuspended in 100 uL DEPC-treated water, and normalized for equal amounts of RNA across samples. Anti-BrdU agarose beads (Santa Cruz Biotechnology) were prepared by washing with Binding Buffer (0.25 X SSPE; 1 mM EDTA; 0.05% Tween 20 (Thermo Fisher Scientific); 37.5 mM NaCl) for 3 min at 4°C three times. Anti-BrdU beads were blocked with Blocking Buffer (Binding Buffer + 0.1% polyvinylpyrrolidone + 500 ug UltraPure BSA (Invitrogen Ambion)) on a rotator for 2 h at 4°C, Blocking Buffer removed and washed twice with Binding Buffer, and resuspended in 400 uL Binding Buffer. RNA was heated at 65°C for 5 min to remove secondary structure, cooled on ice for 2 min, then added to Anti-BrdU beads + Binding Buffer and placed on a rotator for 1 h at 4°C. Beads were then washed sequentially, once with each of the following buffers: Binding Buffer; Low Salt Buffer (0.2X SSPE, 1 mM EDTA, 0.05% Tween 20, DEPC-treated water); High Salt Buffer (0.25X SSPE, 1 mM EDTA, 0.05% Tween 20, 100 mM NaCl), and twice with TET Buffer (0.05% Tween 20 in TE buffer). 250 uL Elution Buffer (20 mM DTT, 150 mM NaCl, 50 mM Tris-HCl, 1 mM EDTA, 0.1% SDS) was then added, gently mixed, and placed in a 42°C water bath for 5 min. Samples were centrifuged to remove beads, and supernatant transferred to a 2 mL tube on ice. An additional 250 uL Elution Buffer was added to the beads for maximal recovery, incubated and centrifuged

as in the last step, and the supernatant added to the tube on ice (total volume of 500 uL). RNA was then precipitated by the addition of 32 uL 5 M NaCl, 1.25 mL ice cold 100% ethanol and 2 uL 20 mg/mL glycogen, gentle mixing, and incubating overnight at -20°C. The next day, samples were centrifuged for 20 min at 20,000 *g* at 4°C. The pelleted RNA was then washed once with 70% ethanol and resuspended in 15 uL DEPC-treated water. cDNA was prepared by adding 2 uL of eluted nascent RNA to 6 uL 5X iScript reaction mix (Bio Rad), 1.5 uL iScript reverse transcriptase (Bio Rad), 20.5 uL Nuclease-free water (Bio Rad), and incubating at 25°C for 5 min, then 42°C for 30 min, then 85°C for 5 min. Sample was then diluted by adding 70 uL DEPC-treated water to cDNA reaction for a total volume of 100 uL. 5uL of each sample was used in each RT-qPCR reaction, with reaction concentrations and qPCR conditions as described previously (ChIPseq). Samples were normalized to the RNAPI-transcribed 25S rRNA.

2.8 RNA extractions

Samples were grown to log phase in SC media and harvested by centrifugation at 3000 *g* for 3 min at 4°C, washed once with AE Buffer, resuspended in 1 mL AE Buffer and transferred to a 1.5 mL tube. Samples were then centrifuged for 10 s at 16,000 *g*, supernatant removed, and remaining pellet resuspended in 400 uL AE Buffer, 40 uL 10% SDS and 440 uL phenol pH 4.5. Samples were mixed thoroughly and subjected to two freeze/thaw cycles: 5 min in -80°C ethanol; 5 min in 65°C water bath, 1 min vortex in between cycles. Samples were frozen one more time in -80°C ethanol bath and centrifuged at 16,000 *g* for 7 min at room temperature. Aqueous layer was transferred to a new tube, to which 1.5X volumes of 1:1 phenol/chloroform was added, mixed, and centrifuged at 16,000 *g* for 5 min. RNA was precipitated by adding sodium acetate (0.14 M, pH 5.2) and 2.5X chilled 100% ethanol, left on ice for 15-45 min, and centrifuged at 20,000 *g* for 2 min at 4°C. Precipitated RNA was washed once with 70% ethanol,

and, after the pellet dried sufficiently, resuspended in 100 uL DEPC-treated water. For each reaction, RNA was DNAsed by combining 24 ug RNA, 20 uL DNAse Buffer I (New England Biolabs), 2 uL DNAse I (New England Biolabs) and DEPC water in a total reaction volume of 200 uL and incubating at 37°C for 10 min. 2 uL of 0.5 M EDTA, pH 8 was then added, and reaction heated to 75°C for 10 min to quench. To prepare cDNA, ~72 ng (in a volume of 6 uL) of DNAsed RNA was added to 16.5 uL Nuclease-free water (Bio Rad), 6 uL 5X iScript reaction mix (Bio Rad) and 1.5 uL iScript reverse transcriptase and incubated at 25°C for 5 min, then 42°C for 30 min, then 85°C for 5 min. Sample was then diluted 30X in DEPC-treated water. 5 uL of each sample was used in each RT-qPCR reaction, with reaction concentrations and qPCR conditions as described previously (ChIPseq). Samples were normalized to the RNAPI-transcribed 25S rRNA.

2.9 Transformations

10 mL of the receiving strain was grown to log phase in YPD, centrifuged at 3000 *g* for 5 min at room temperature, washed once with an equal volume of sterile water. The pellet was resuspended in 500 uL 0.1 M LiAc, transferred to a 1.5 mL tube, and centrifuged at 16,000 *g* for 15 s. The supernatant was removed, and the pellet resuspended again in 500 uL 0.1 M LiAc. For each transformation, 100 uL of resuspended pellet was centrifuged, supernatant removed, and mixed with 240 uL 50% PEG 3500, 36 uL 1 M LiAc, 25 uL boiled SS-carrier DNA, 30 uL sterile water, and 20 uL PCR cassette containing tag/replacement gene and selectable marker. Transformation mixes were incubated at 42°C for 20-40 min, centrifuged at 16,000 *g* for 30 s, supernatant removed, and pellet resuspended in 80 uL sterile water. The resuspended pellet was then plated on drop-out media as required and incubated at 30°C for 2 to 3 days.

2.10 Yeast Media

Strains were grown primarily in either YPD (1% yeast extract; 2% peptone; 2% glucose) or Synthetic Complete (SC) media (0.17% YNB; 0.5% ammonium sulfate; 2% glucose). "Drop-out" media that is deficient in a particular amino acid (a formulation of SC media) was also used to select for transformants that successfully integrated the desired target into the *S. cerevisiae* genome.

2.11 Quick Yeast Protein Extract

Cells were grown overnight in YPD in a 30°C shaker until they reached saturation the next morning. 1mL of culture was then transferred to a 1.5mL tube, centrifuged for 1 min at top speed, then supernatant removed. The pellet was resuspended in 1mL ice-cold dH_2O, to which 150uL of YEX buffer (1.85 M NaOH; 7.5% 2-mercaptoethanol) was added, and the tube left on ice for 10 min. 150uL of 50% TCA (trichloroacetic acid) was then added to the tube and left on ice for 10 min, with occasional tapping of the tube. The tube was then centrifuged at 20,000 *g* at 4°C for 5 min, and then the supernatant removed. The pellet was resuspended in 100uL 2X Sample Buffer (140 mM Tris-HCl, pH 6.8; 4% SDS; 20% Glycerol; 0.02% bromophenol blue), and then 1M Tris pH 8.0 added dropwise until sample turned to blue to appropriately adjust pH. The tube was then boiled for 5 min at 95°C and stored at -20°C.

Section 3: Results

3.1 Rpb1 is sumoylated under normal growth and under stress conditions

3.1.1 Rpb1 is sumoylated under normal growth

Whereas previously published work demonstrated that Rpb1 is sumoylated only following UV-stress (Chen et al., 2009), work in our lab has shown repeatedly that Rpb1-sumoylation can be detected under normal growth (Travas, 2021). This result was confirmed by a Western Blot that was conducted on an Rpb1-enriched protein lysate. Western Blot is a common method of detecting sumoylated substrates, whereby proteins in a given sample are first separated by size through an SDS-PAGE gel, immunoblotted with an antibody that specifically binds SUMO, and then imaged by chemiluminescence. To enrich for specific proteins prior to Western Blotting (rather than imaging all sumoylated substrates), samples are typically first immunoprecipitated (IP'd) by incubating the lysate with an antibody that targets the protein of interest, such as Rpb1 (see Section 2.2 for details). Figure 4 shows an experiment where Rpb1 was IP'd from wild-type (WT) cells and immunoblotted for SUMO. As a sumoylated band can clearly be seen in the W303a lane, this experiment establishes that Rpb1 is sumoylated during normal growth.

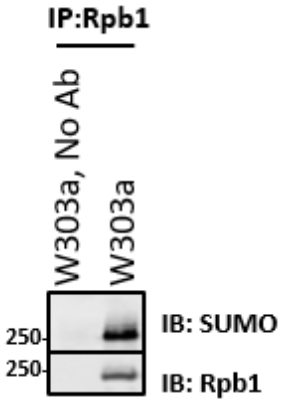

Figure 4: Sumoylation of Rpb1. Western Blot of IP'd Rpb1 in a wild-type strain (W303a). Lysate was immunoblotted with Rpb1 and SUMO, indicating sumoylation under normal growth conditions. Figure adapted from Travas (2021).

3.1.2 Sumoylated Rpb1 is mostly on chromatin

Though Rpb1 has now been established to be sumoylated during normal growth, it remains unclear what function this Rpb1-modification plays. But as transcription-associated proteins constitute one of the largest groups of SUMO substrates (Vertegaal, 2022), my hypothesis is that sumoylated Rpb1 plays a role in active transcriptional processes during normal growth. Because chromatin-associated proteins are important components of gene expression regulation (Cuevas-Bermúdez et al., 2019), one way to parse the role of sumoylated Rpb1 is to examine the relative amounts of sumoylated and unsumoylated Rpb1 that are either associated with chromatin, or freely soluble in the cell. If the amount of Rpb1 that is sumoylated is greater in the chromatin-associated fraction of the cell than in the soluble portion, this would imply a stronger requirement for sumoylated Rpb1 that is actively involved in transcription, as opposed to Rpb1 that could be dispersed throughout the nucleoplasm (Zeng et al., 1997) or in the cytoplasm, where the RNAPII subunits are assembled prior to nuclear import (Wild & Cramer, 2012).

To examine this, a chromatin fractionation and subsequent Western Blot was conducted. The chromatin fractionation process involves centrifugation of the sample lysate under osmotic conditions that pellet chromatin-associated proteins. This produces two fractions: a soluble fraction (the supernatant), and a chromatin-associated fraction (the pellet, resuspended). Typically, detection of a specific sumoylated protein in fractionated lysates requires the use of a substrate-specific antibody (rather than using a SUMO antibody), following which the sumomylated form can be detected as a slightly heavier band (than the unsumoylated form) in a Western Blot. However, this method relies on using antibodies that are sensitive enough to reliably parse and quantify the sumoylated form from the unsumoylated form of the substrate, which can be difficult for both larger proteins (where the weight of a SUMO group is a smaller

fraction of the total weight, compared to smaller proteins), as well as those where the sumoylated population is expected to be quite small. For these reasons Rpb1, analysts in our lab, including myself, have often found detecting sumoylated-Rpb1 in an Rpb1 immunoblot a challenge. One way to solve this, by eliminating the contribution of unsumoylated Rpb1 and generally simplify the process, I performed an Rpb1-IP of the fractionated lysates to first enrich the sample, and then immunoblot with the SUMO antibody. Immunoprecipitating Rpb1 allows for the use of the SUMO antibody, since other sumoylated proteins should not be illuminated in the Western Blot.

Figure 5 shows an immunoblot of a chromatin-fractionated WT sample that was IP'd with Rpb1. The lower regions of the blot show antibody controls that detect the nucleosome-associated H3 histone (H3) and glyceradehyde 3-phosphate dehydrogenase (GAPDH), which is prodominantly found in the cytoplasm (Tristan et al., 2011). Remarkably, the ratio of sumoylated Rpb1 (IB:SUMO) to total Rpb1 (IB:Rpb1) shows that a significantly greater proportion of chromatin-associated Rpb1 is sumoylated than soluble Rpb1 (Figure 5B), implying an involvement in transcriptional processes.

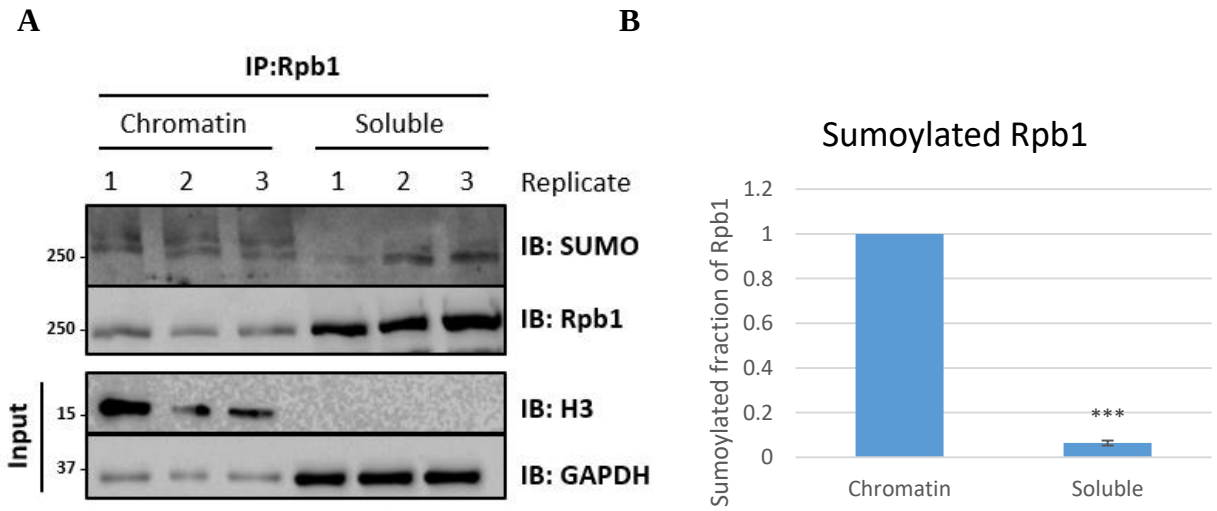

Figure 5: Chromatin fractionation of sumoylated Rpb1. (**A)** Western Blot of chromatin-fractionated WT lysates that were IP'd with Rpb1 (input used for H3 and GAPDH), in triplicate. H3 and GAPDH blots represent positive controls for chromatin-associated and soluble lysates, respectively. **(B)** Quantification of SUMO signal normalized to Rpb1 levels. Sumoylated fraction of Rpb1 (y-axis) is scaled for improved readability (Chromatin is scaled to 1.0).

3.1.3 Sumoylation of Rpb1 is transient, and rapidly deconjugated by Ulp1

Like ubiquitination, sumoylation is a dynamic process that involves the interplay of both conjugating and deconjugating enzymes. Because the dynamics of SUMO proteases are varied and context-dependent (Hickey et al., 2012; Celen & Sahin, 2020), understanding how they mediate the regulation of Rpb1-sumoylation could offer valuable insight into their functional role for Rpb1. Indeed, it was recently reported that sumoylation is remarkebly transient for most targets. It is currently unclear why SUMO conjugation requires the rapid "on/off" cycling, but it has been suggested that this may facilitate other dynamic processes, such as multivalent interactions of the SUMO target, or perhaps help stabilize these often disordered regions (McNeil et al., 2024). Given Rpb1 undergoes considerable modifications (including sumoylation) at its disordered linker region and CTD (see Section 1.2, 3.3), this is an intriguing model for Rpb1, and the dynamics thus worth exploring as we may expect to also see rapid sumoylation/desumoylation for this large subunit of RNAPII.

To determine how quickly Rpb1 sumoylation is deconjugated, 1,10 Phenanthroline was applied to a WT strain (*ULP1*) as well as a Ulp1-impaired strain (*ulp1-mt*) to block sumoylation. 1,10 Phenanthroline is a metal chelator that has been shown to sequester zinc and inhibit metal-dependent enzymes (reviewed in Nam, 2021). It also has been recently used in our lab to quickly and effectively reduce the level of global de novo sumoylation in yeast (McNeil et al., 2024). Because SUMO-substrate linkages are primarily deconjugated by Ulp1, it is expected that 1,10 Phenanthroline will not appreciably reduce Rpb1-sumoylation in the *ulp1-mt* strain, given it appears to only block de novo sumoylation. *ULP1* and *ulp1-mt* cultures were grown to log phase, administered 500ug/mL of 1,10 Phenanthroline and harvested at 3 min and 10 min post-application. Figure 6 shows that as soon as three minutes after application, Rpb1-sumoylation is virtually undetectable in the *ULP1* strain, indicating rapid deconjugation. Conversely, persistant

Rpb1-sumoylation in the *ulp1-mt* strain at all time points confirms Ulp1 as the primary agent of Rpb1-desumoylation.

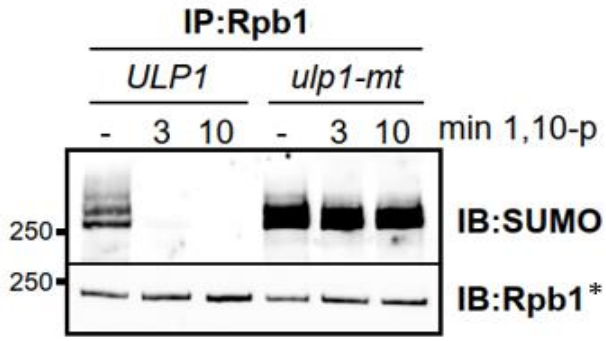

Figure 6: Dynamic sumoylation of Rpb1. Western Blot of Rpb1-IP in WT (*ULP1*) and Ulp1-impaired (*ulp1-mt*) strains before and after 1,10 Phenanthroline treatment, immunoblotted with SUMO and Rpb1 antibodies. *Note that for the Rpb1 loading control, an antibody recognizing the N-terminal region of Rpb1 was used (see materials and methods), instead of the 8WG16 antibody that was used in the majority of this thesis work.

3.2 Characterization of Ulp2-dependent Rpb1 sumoylation

3.2.1 Blocking the proteasome does not stabilize sumoylation in *ulp2Δ*

Recall from the introduction that Ulp2 is the primary SUMO protease involved in reducing SUMO-SUMO bonds that accumulate on sumoylated substrates (Hickey et al., 2012; Eckhoff & Dohmen, 2015; Bylebyl et al., 2003). As expected, a global increase high-molecular weight SUMO conjugates is a well-established consequence of Ulp2 null-mutants (*ulp2Δ*), as compared to wild-type cells (*ULP2*) (Bylebyl et al., 2003; Li & Hochstrasser, 2000). Accordingly, one may reasonably expect to see elevated levels of sumoylated Rpb1 in *ulp2Δ* cells. Interestingly, however, previous work by E. Rosonina (unpublished results) shows that sumoylated Rpb1 levels in fact appear reduced in a *ulp2Δ* background, compared to *ULP2* (Figure 7A).

It was previously reported that Ulp2 functions to protect some substrates from degradation that occurs via the ubiquitinating heterodimer ligase Slx5/Slx8 (Psakhye et al., 2019; Uzunova et al., 2007). This heterodimer ligase is part of a larger family of SUMO-Targeted

Ubiquitin Ligases (STUbLs) that function to ubiquitinate sumoylated substrates and regulate their activity in various ways, including substrate degradation (Chang et al., 2021). We thus considered the possibility that the reduced levels of sumoylated Rpb1 observed in the *ulp2Δ* strain were a consequence of excessive polysumoylated Rpb1 being targeted by the proteasome and ultimately degraded (Figure 7B). Indeed, in the related ubiquitin system, while mono-ubiquitinated proteins can be quite stable, proteins with chains of attached ubiquitin are more susceptible to degradation (Matunis et al., 1998).

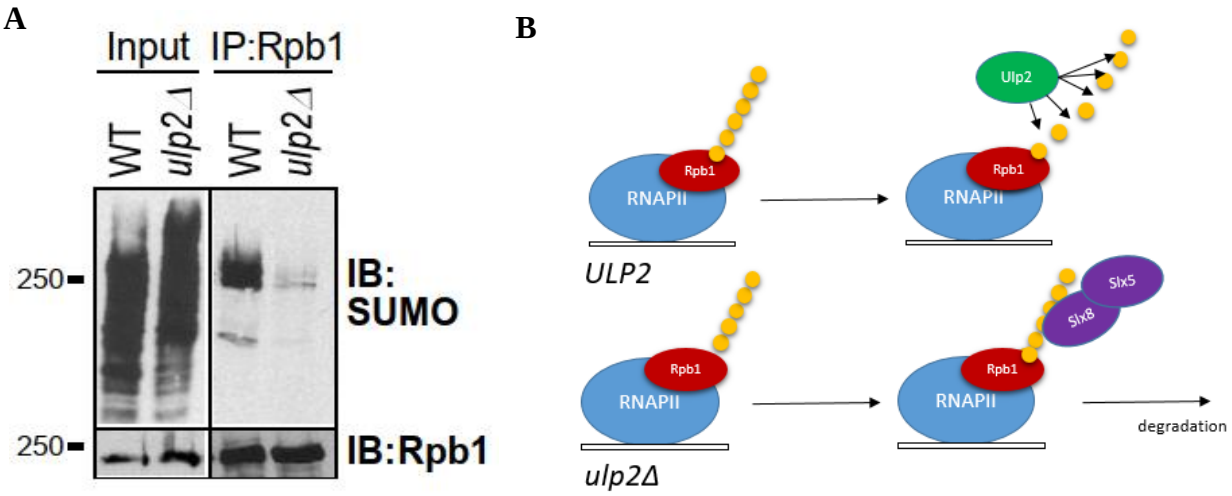

Figure 7: RNAPII sumoylation depends on Ulp2. (A) Western Blot of Rpb1-IP (and input) in WT and *ulp2Δ* strains, immunoblotted with Rpb1 (E. Rosonina, unpublished data). **(B)** Model of Rpb1 sumoylation in *ulp2Δ* strain. As Ulp2 cleaves polysumoylation in a *ULP2* strain (upper), SUMO chain buildup on Rpb1 in a *ulp2Δ* background leads to Slx5/Slx8-mediated Rpb1 degradation (lower).

To examine this possibility, we applied the proteasomal inhibitor MG132, a peptide aldehyde that blocks the active site of the proteasome (Kisselev et al., 2012; Lee et al., 1998), to *ULP2* and *ulp2Δ* strains and examined sumoylated Rpb1 levels. We expected that, if by blocking proteasomal activity, degradation of polysumoylated Rpb1 was reduced, the stabilized sumoylated Rpb1 signal could be detected by Western Blot. Cultures were treated with 10mg/mL

of MG132 for 30 min, IP'd with Rpb1 and immunoblotted. As Figure 8A shows no appreciable increase in sumoylated Rpb1 in MG132-treated *ulp2Δ* (compared to *ulp2Δ* not treated with MG132), blocking the proteasome does not appear to rescue polysumoylated Rpb1 from degradation in the *ulp2Δ* strain. This suggests that the observed decrease in sumoylated Rpb1 in the *ulp2Δ* strain is not due to degradation by the proteasome.

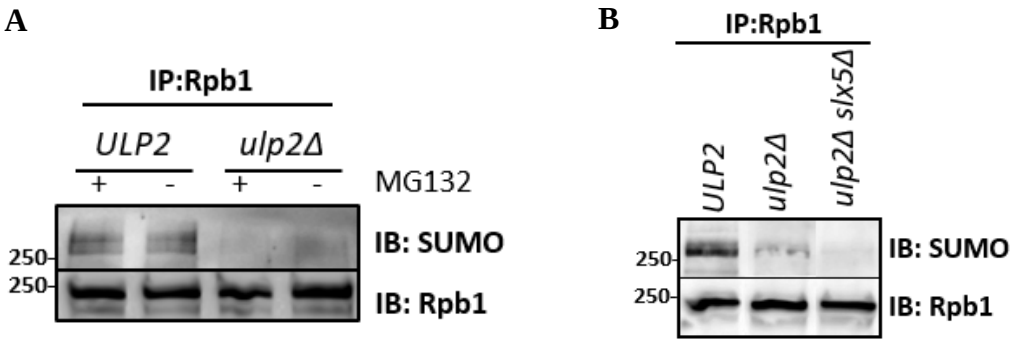

Figure 8: Reduced Rpb1 sumoylation in *ulp2Δ* does not appear to involve the proteasome. (**A)** Western Blot of IP'd Rpb1 with and without the proteasome-inhibitor MG132 (30 min), in WT (*ULP2*) and *ulp2Δ* strains. **(B)** Western Blot of IP'd Rpb1 in WT (*ULP2*), *ulp2Δ*, and *ulp2Δ-slx5Δ* strains. Note that the uneven background colouration between lanes is a result of rearranging the original image (loading order) for clarity.

3.2.2 Deleting *SLX5* does not stabilize Rpb1 sumoylation in *ulp2Δ*

Operating under the hypothesis that polysumoylated Rpb1 is targeted for Slx5/Slx8-mediated degradation (Figure 7B), it is unclear why blocking the proteasome did not stabilize polysumoylated-Rpb1 (Figure 8A). To investigate further, an orthogonal approach was developed to directly compromise this degradation pathway by deleting the *SLX5* gene, thereby removing this ubiquitin ligase. Deleting *SLX5* would thus be expected to inhibit ubiquitination and subsequent degradation of polysumoylated Rpb1, potentially preserving these conjugates. Accordingly, a *ulp2Δ-slx5Δ* strain was generated.

As described in 3.2.1, *ULP2*, *ulp2Δ* and *ulp2Δ-slx5Δ* strains were IP'd with Rpb1 and immunoblotted with SUMO and Rpb1 (Figure 8B). Because the deletion of *SLX5* shows no rescue of Rpb1 sumoylation, the mechanisms behind Ulp2-dependent Rpb1 sumoylation and

consequent reduction of Rpb1 sumoylation in the absence of Ulp2 remain unclear, but appear not to involve ubiquitin- and proteasome-mediated degradation.

3.3 Rpb1 is sumoylated at K1487

3.3.1 RNAPII sumoylation is on Rpb1

It was previously shown that the primary site of Rpb1 sumoylation under UV-stress is K1487 (Chen et al., 2009). Having now shown that Rpb1 sumoylation occurs under normal growth conditions (Figure 4), an experiment was conducted to confirm that K1487 is also the primary site of sumoylation during normal growth. To do this, an Rpb1-IP and subsequent immunoblot was performed with a WT strain, as well as a previously constructed strain that replaced Lys-1487 with Arg (K1487R). Figure 9 shows that in the K1487R mutant, Rpb1 sumoylation is significantly reduced (though not abolished), confirming this to be a major site of Rpb1 sumoylation during normal growth conditions.

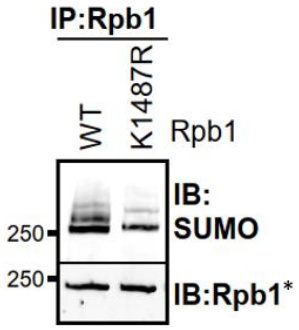

Figure 9: Rpb1 sumoylation is mostly at K1487. (A) Western Blot of Rpb1-IP'd WT and the sumoylation-impaired K1487R strains, immunoblotted with SUMO and Rpb1. *Note that for the Rpb1 loading control, an antibody recognizing the N-terminal region or Rpb1 was used, instead of the 8WG16 antibody that was used in the majority of this thesis work.

3.3.2 K1487R exhibits normal growth

To determine if the K1487R mutant has any associated growth defect that may signal transcriptional compromise, growth assays were performed in rich media (YPD). Using saturated overnight cultures as starting inoculum, liquid cultures were inoculated in triplicate and grown at

30ºC in the accuSkan spectrophotometer to measure growth rates for each strain (Figure 10A & B). Using the same starting inoculum, spot assays were also performed to measure growth on solid media (Figure 10C). These growth studies show that the K1487R strain exhibits no growth impairment as compared to the WT strain. This is perhaps not unexpected given previous work showed that a sumoylation-impaired Tfg1 - the most sumoylated subunit of TFIIF, to which half of all RNAPII molecules are complexed with - also did not show any growth impairment (Baig et al., 2021). Indeed, it suggests that mutating even major sumoylation sites of crucial components of the transcriptional machinery may not appreciably affect growth under normal conditions.

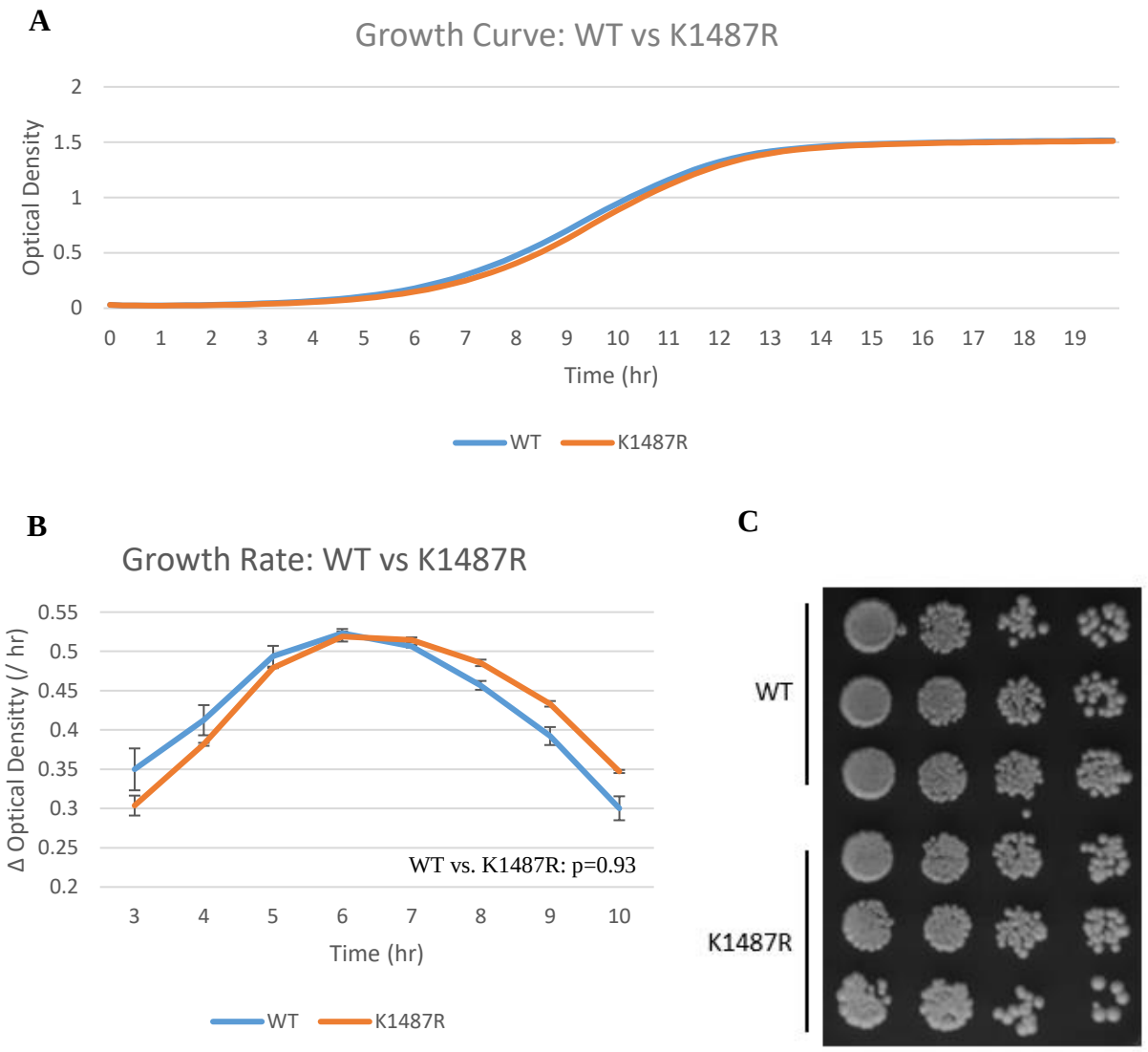

Figure 10: K1487R mutation does not impact growth. (A) Growth curves showing WT and K1487R culture densities as measured by the accuSkan spectrophotometer in YPD media. **(B)** Growth rates calculated from timepoints from **(A)** during exponential growth. ODs were ln-transformed to generate per-hour growth rates and calculate error bars (SEM) and overall p-value. **(C)** Spot assay of WT and K1487R strains at 30°C after 2 days growth on YPD media, in triplicate.

3.3.3 The SUMO status of Rpb1 does not impact association with Spt6

Spt6 is a transcription factor and nucleosome remodeler that has long been implicated in a number of transcriptional processes such as mRNA processing, histone modification, and nucleosome reassembly (Sdano et al., 2017). While it was originally thought to bind the CTD of Rpb1, Spt6 was recently shown to bind at specific phosphorylated residues that lie in the Rpb1 linker region, notably S1493, T1471 and Y1473 (Sdano et al., 2017). Given the close proximity

of these residues to the major Rpb1 sumoylation site (Figure 11A), we developed an experiment to explore whether sumoylation at K1487 plays a role in an interaction of Rpb1 with Spt6. It would be expected that an observed increase in Rpb1/Spt6 association in the K1487R strain may suggest that Rpb1 sumoylation plays an inhibitory role in this interaction, whereas a decrease may suggest Rpb1 sumoylation facilitates this interaction in some way.

To examine this, we first HA-tagged the *SPT6* gene in both WT and K1487R strains so we could then IP Rpb1 in each strain and examine associated Spt6-HA levels by immunoblot. HA (human influenza hemagglutinin) is a commonly used epitope tag in *S. cerevisiae* that is useful for manipulating and examining the behavior of a target protein, and which can be integrated via homologous recombination (Wang et al. 2017). To HA-tag Spt6, we used a well-established method described by Knop et al. (1999) and many others elsewhere in the literature. Briefly, the HA-tagged cassette and associated auxotrophic marker are amplified using primers that are designed with extended 5' sequences which carry homology to the target site of integration (Figure 11B). The PCR product is then transformed into competent yeast cells and plated on SC-TRP, which is selective media upon which only cells that have successfully integrated the cassette containing the selective marker should grow. Colonies were then screened by PCR (Figure 11C) to confirm genetic integration, and then expression of the Spt6-HA product was confirmed by Western Blot (Figure 11D).

Following successful generation of the *SPT6-HA* cassette in both the WT and K1487R strains, whole protein lysates from each strain were prepared, IP'd with Rpb1, and immunoblotted with HA and Rpb1. The Western Blot in Figure 11E shows that despite its close proximity to Spt6 binding sites, the K1487R mutation does not appear to significantly impact the association of Spt6 with Rpb1.

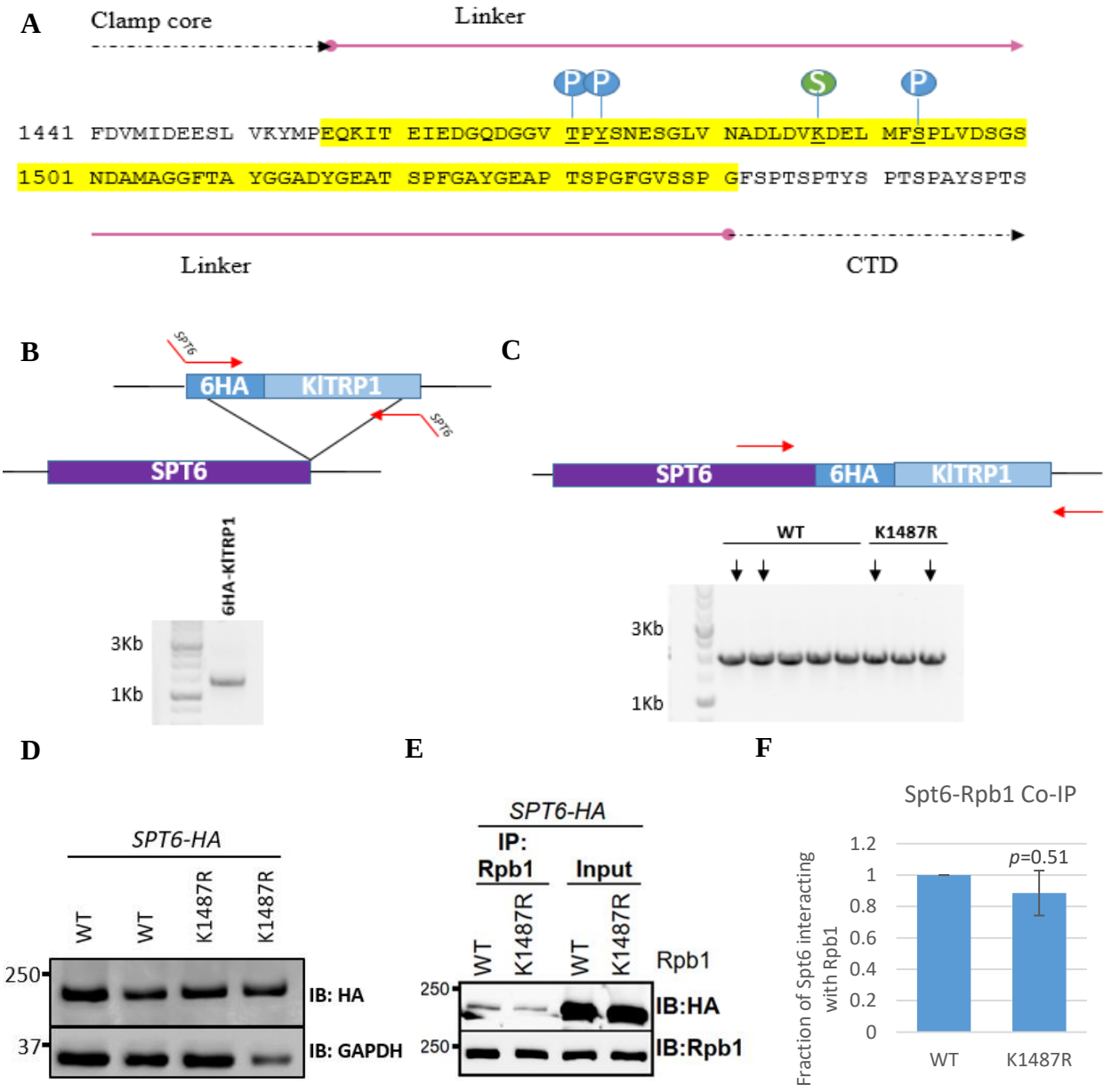

Figure 11: Spt6/Rpb1 interaction in WT and K1487R strains. (**A**) Amino acid sequence of Rpb1-linker region, which is flanked by the Rpb1 Clamp core and the C-terminal domain (CTD) (Cramer et al., 2001), and spans residues 1456-1541 (Sdano et al., 2017). Phosphorylated residues are annotated with a blue "P" and the SUMO site K1487 annotated with a green "S". **(B)** Schematic of primer locations (red arrows), which were designed to have homology with *SPT6* at the 5' end of each for homologous recombination (upper). Agarose gel electrophoresis of the *6HA-KlTRP1* cassette PCR product used for transformation (lower). **(C)** Schematic of the expected *SPT6*-tagged region following transformation, with screening primer locations shown with red arrows (upper). Agarose gel electrophoresis of PCR products showing the expected size (~1900bp) of the integrated product (lower). Black arrows indicate clones chosen to confirm tag expression by Western Blot. **(D)** Western Blot of selected clones from **(C)**, immunoblotting with HA to confirm Spt6-HA expression (GAPDH as loading control). **(E)** Western Blot of HA-tagged Spt6 in WT and K1487R strains, Rpb1-IP'd and immunoblotted with HA and Rpb1. **(F)** Quantification by ImageJ of HA signal normalized to Rpb1 levels for three biological replicates (data not shown for subsequent replicate Western Blots). HA-interacting fraction of Rpb1 (y-axis) is scaled for improved readability (HA/Rpb1 ratio in the WT was scaled to 1.0).

Because no significant impact on the Spt6/Rpb1 interaction was observed in the K1487R strain, when sumoylation at this site is impaired, we next considered an approach that examined the interaction of Rpb1 and Spt6 when Rpb1 sumoylation levels are elevated (beyond those observed during normal growth). Because Rpb1 sumoylation has been reported to significantly increase under UV-stress (Chen et al., 2009), we developed an experiment that examined the Rpb1/Spt6 interaction in WT cells that have been UV-irradiated.

First, to determine at what point Rpb1-sumoylation is maximized following UV-stress, a time course was conducted at two UV intensities. A large culture of WT cells was grown to exponential phase, irradiated with either 50J or 400J UV light, and harvested at four time points: 0, 20, 40, and 60 min following exposure. Intensities and time points were chosen based on the upper and lower ranges used in similar studies (in the literature) that examined the impact of UV-irradiation on Rpb1 sumoylation, Rpb1 stability, and transcriptional reprogramming (Chen et al., 2009; Heckmann et al., 2019; Hauser et al., 2019). Post-exposure cells were then grown both under normal lab lighting and in the dark, since these conditions prompt different repair pathways (Sancar, 2016) and the induction of Rpb1-sumoylation may be greater in one than the other. Cultures were then harvested, IP'd to enrich for Rpb1, and immunoblotted. Figure 12 shows that Rpb1-sumoylation is maximized around 20 min post-recovery, and perhaps at slightly higher levels when recovery occurs in the dark.

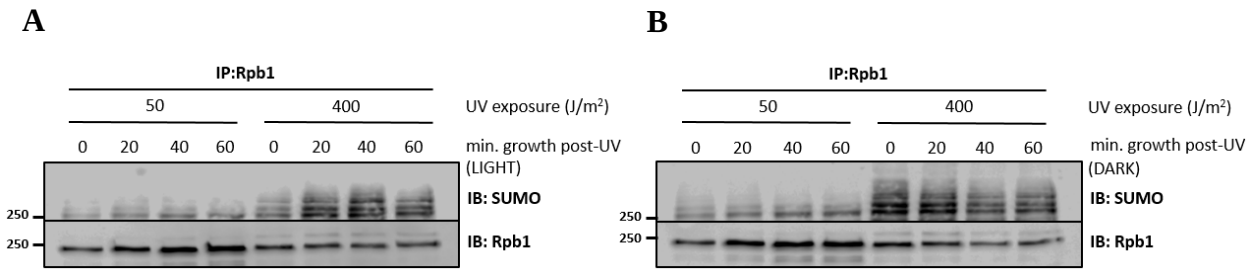

Figure 12: Optimization of UV conditions for maximal Rpb1 sumoylation. Western Blots of Rpb1-IP'd cultures that were grown to log phase and irradiated with either 50J or 400J UV. Following irradiation, cells were grown in a 30°C shaker under either normal lab light conditions **(A)** or where culture tubes were covered with foil **(B)**. Samples were harvested at time intervals 0, 20, 40, and 60 min following irradiation. IP'd lysates were immunoblotted with SUMO and Rpb1 to determine when maximal Rpb1 sumoylation occurs.

Having established optimal UV conditions for maximizing Rpb1 sumoylation, a WT culture was grown to log phase, irradiated with 400J, and harvested following 20 min recovery in a 30°C shaker, where the tube was covered with foil. Cultures were then harvested, IP'd with Rpb1 and subsequently immunoblotted with Rpb1 and Spt6-HA. Figure 13 shows that elevated levels of sumoylated-Rpb1 do not significantly increase or decrease Rpb1 association with Spt6, and consequently this was not pursued further.

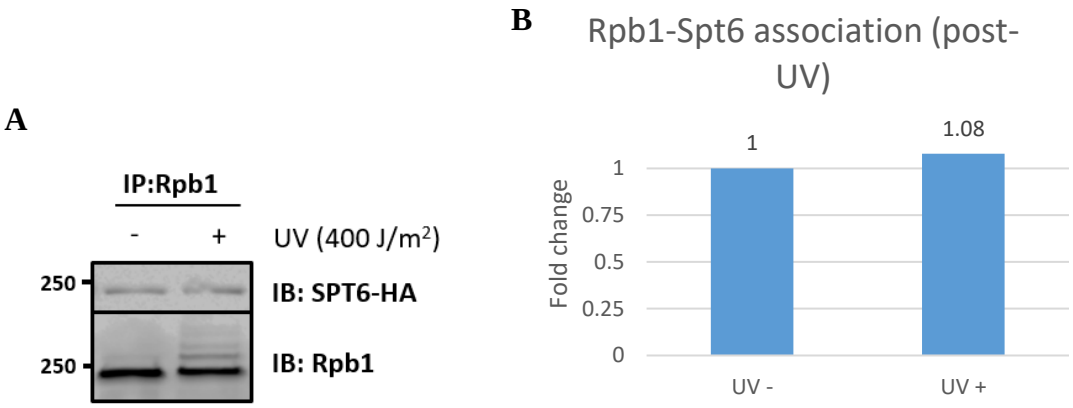

Figure 13: Spt6/Rpb1 interaction in WT cells following UV stress. (A) Western Blot of Rpb1-IP'd WT cells with and without 400J UV irradiation. Post-irradiation cultures were grown in the dark for 20 min prior to harvesting. IP'd cells were immunoblotted with HA and Rpb1. **(B)** Quantification by ImageJ of HA signal normalized to Rpb1 levels. HA-interacting fraction of Rpb1 (y-axis) is scaled for improved readability (HA/Rpb1 ratio in WT was scaled to 1.0). Error bars not included, as only one replicate was completed.

3.3.4 K1487R exhibits increased nascent transcription at a small subset of genes, including several stress genes during normal growth

Thus far, despite the finding that Rpb1-sumoylation largely occurs at K1487, the Rpb1-K1487R mutant has shown no impairment with regard to growth or interaction with the nucleosome remodeler Spt6. However, because these observations of growth and Spt6-interaction serve as indirect indicators of transcriptional processes, the question remains to what extent does sumoylation at Rpb1-K1487 regulate transcriptional activity, if at all? To address this question, a whole-genome transcriptional assay was conducted to examine potential differences in mRNA levels between the wild-type and Rpb1-K1487R mutant strains. And in an effort to minimize the potentially confounding effects of steady state mRNA regulatory processes that act degrade mRNA (O'Brien et al., 2023), a specialized method of RNAseq was performed, called GROseq (Global run on sequencing), which is based upon the method developed by Al-Husini et al. (2017), and targets only nascent transcripts. GROseq examines nascent RNA transcripts by labeling newly synthesized RNA with brominated UTP (BrUTP), followed by a BrUTP-IP to enrich for nascent RNA. Differential analysis of the nascent RNA can then be performed to determine what genes (if any) are differentially expressed in the K1487R strain.

In this experiment, GROseq was performed on two biological replicates during normal growth for both the WT and K1487R strains. 24 genes were identified as differentially expressed (FDR 0.05), with 22 genes showing increased expression in the K1487R strain, and 2 decreased expression (Figure 14). Remarkably, more than one quarter of the upregulated genes are associated with the stress response, including *DDR2*, *RCK1*, *HSP26*, *IKS1* and *CTT1* (Figure 14B). Figure 15 shows coverage plots for two such stress genes, *HSP26* and *DDR2*, where a clear upregulation of nascent RNA in the K1487R strain can be seen (A), as well as a selection of genes with unchanged expression (B).

A

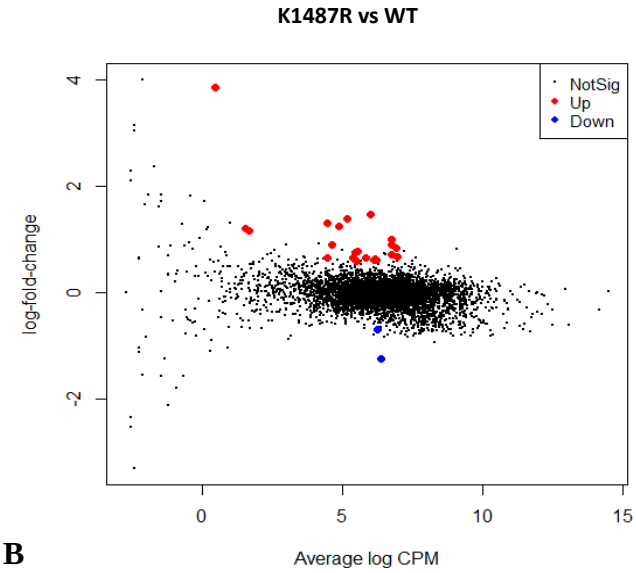

B

Genes	logFC	logCPM	FDR	Description
YGR161W-B	3.860110893	0.4558	5.26E-07	Retrotransposon TYA Gag and TYB Pol genes
HSP26	1.479301984	6.016747	0.002878	Small heat shock protein (sHSP) with chaperone activity
DDR2	1.389677556	5.155907	1.16E-13	Multi-stress response protein
RCK1	1.302070806	4.448632	2.77E-09	Protein kinase involved in oxidative stress response
LEE1	1.246174687	4.898494	7.09E-10	Zinc-finger protein of unknown function
PAU24	1.208906358	1.567808	0.031525	Cell wall mannoprotein
YBR072C-A	1.176620046	1.669423	0.03228	Putative protein of unknown function
CTT1	1.005783809	6.747869	0.030466	Cytosolic catalase T
YLR326W	0.911663456	6.779593	0.017665	Putative protein of unknown function
YFL002W-A	0.905183908	4.628246	0.000164	Retrotransposon TYA Gag and TYB Pol genes
IRC8	0.849807345	6.925768	0.000661	Bud tip localized protein of unknown function
YOR192C-C	0.777936632	5.548805	0.002043	Putative protein of unknown function
IMA2	0.76091281	5.453654	0.000661	Isomaltase (alpha-1,6-glucosidase/alpha-methylglucosidase)
IKS1	0.722586451	6.740517	0.008723	Protein kinase of unknown cellular role
DAN4	0.670326461	6.951529	0.03228	Cell wall mannoprotein
CRC1	0.664804808	4.463705	0.036493	Mitochondrial inner membrane carnitine transporter
HXT11	0.653877644	5.846126	0.008723	Hexose transporter
FMP45	0.648203453	5.396386	0.010445	Integral membrane protein localized to mitochondria
YJL132W	0.640968572	6.178419	0.014997	Putative protein of unknown function
AGX1	0.62396311	6.225338	0.033664	Alanine:glyoxylate aminotransferase (AGT)
CTR3	0.620269625	6.137691	0.03228	High-affinity copper transporter of the plasma membrane
YDR215C	0.591579358	5.508424	0.03228	Putative protein of unknown function
snR70	-0.681245738	6.264324	0.017665	C/D box small nucleolar RNA (snoRNA)
BSC1	-1.237879189	6.39856	0.000941	Protein of unconfirmed function

Figure 14: GROseq differential expression between WT and K1487R. (A) Scatterplot of genes identified in the K1487R strain as having increased expression (red dots) and decreased expression (blue dots) by GROseq. Fold change (log2) is plotted against read density. **(B)** Genes identified as differentially expressed (FDR < 0.05), ranked by fold change (log2). Genes highlighted in orange are associated with the environmental stress response (ESR) (Gasch et al. (2000)) or elsewhere identified as stress response genes (Bilsland et al., 2004; Kobayashi & McEntee, 1990).

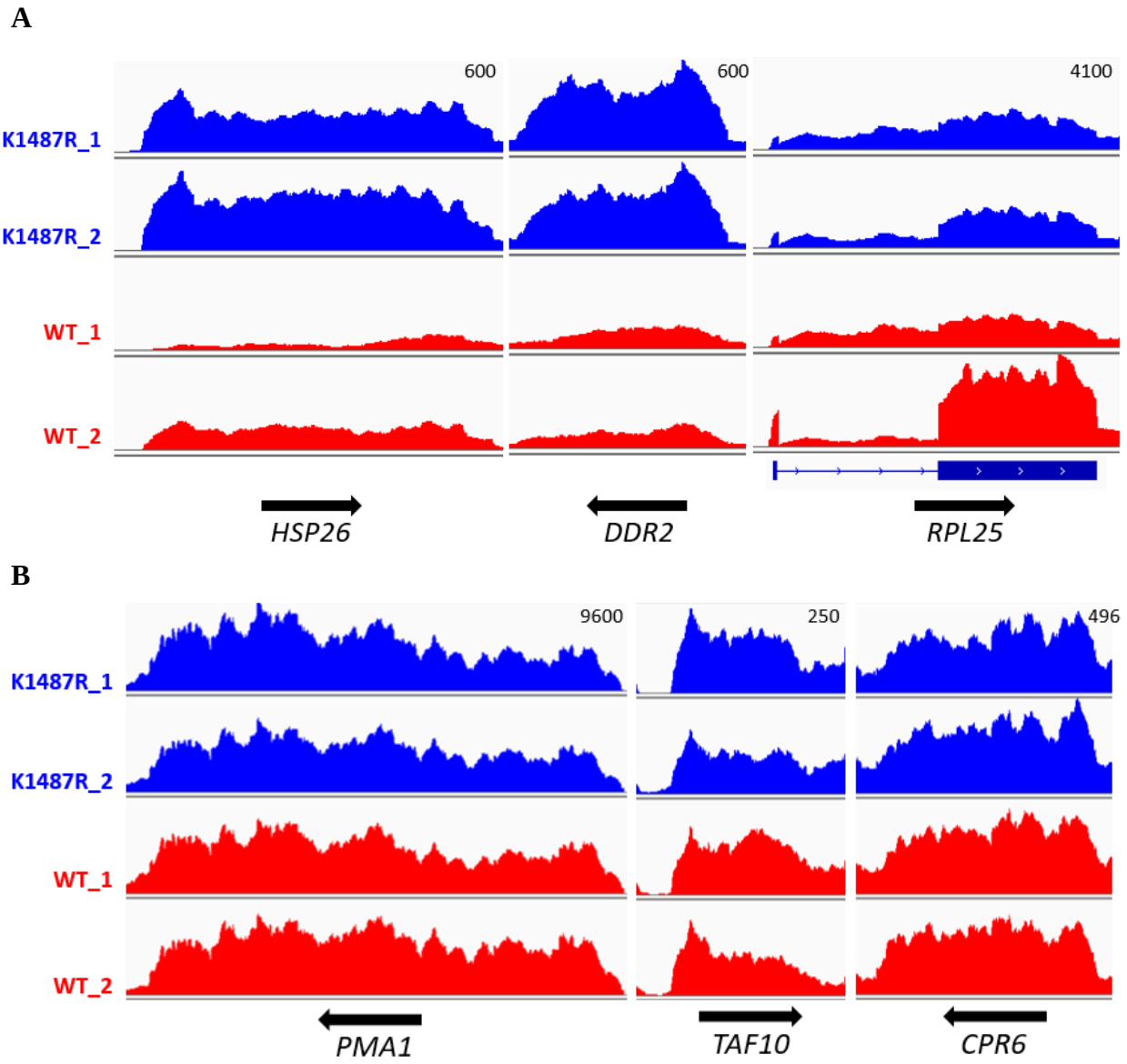

Figure 15: Read coverage alignments for select genes: Unnormalized GROseq read coverage alignments for RNAPII in WT and K1487R samples for: **A)** Stress genes (*HSP26*, *DDR2*) and a ribosomal gene with an intron (*RPL25*). For *RPL25*, intron is demarcated by the gapped-region of the blue bar at the bottom of the figure; **B)** Constitutively expressed genes *PMA1*, *TAF10* and *CPR6*, showing relatively unchanged expression levels. Images for all genes were generated in IGV. Numbers in the top right corner of each alignment indicate range of read coverage.

It is important to note that before performing the differential analysis, a multidimensional scaling analysis (MDS) of the sequenced samples was done to assess the quality of the sequenced data. This MDS plot reduces the dimensionality between each sample (across thousands of genes) to the two most consequential dimensions, and the distance between replicates on the plot correlates to their dissimilarity. It is a fairly abstract plot, but essentially, if

replicates group together it generally means most of the differences are between strains rather than replicates, which is one indication of good quality data (Ritchie et al., 2015). The plot in Figure 16 shows that though the K1487R strains clustered well, the WT samples did not group together as well.

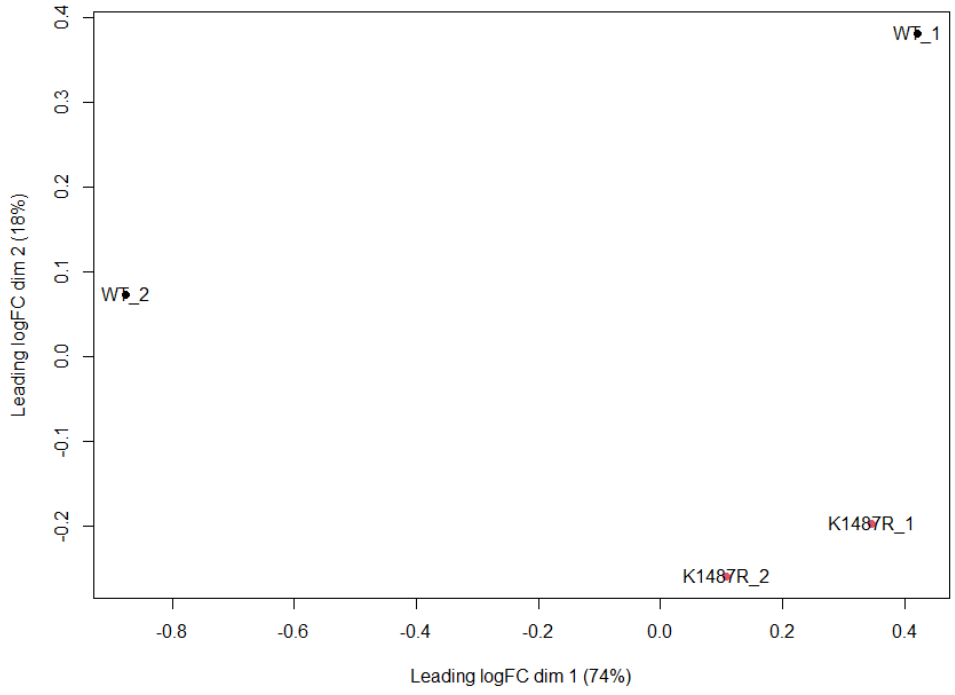

Figure 16: Clustering of WT and K1487R GROseq data. (A) Multidimensional scaling plot showing normalized GROseq counts. Samples were clustered using the plotMDS function in the bioinformatics tool edgeR to show correlation between samples. The x- and y-axes approximate the first and second largest sources of variability within the data, respectively.

To investigate these differences, we scanned through the coverage profiles (read coverage) for each sample in the Integrated Genomic Viewer (IGV), which revealed some differences at specific genes between the WT replicates. For instance, genes with introns show significantly more spliced fragments in the second WT replicate. Because nascent transcripts would be expected to undergo less processing (such as splicing) than mature mRNA, we would expect to see more intron sequences in GROseq data than in typical RNAseq. The intron-

containing *RPL25* is shown in Figure 15A, where a large difference between coverage within intron and exon regions can be seen for this replicate (WT_2). This suggests that this replicate may not have been as enriched for nascent transcripts as the other samples, implying perhaps a larger fraction of mature RNA was sequenced. It is possible this could be due to a technical error that caused higher background RNA in the sample preparation, potentially accounting for the weak clustering of the WT samples in the MDS plot above. Unfortunately, because at least two samples are required in order to conduct a robust differential analysis, the increased variability in the WT replicates potentially obscured more subtle differences between WT and K1487R strains that would otherwise have been detected in WT replicates that were better correlated with each other.

3.3.5 Validation of GROseq results

RT-qPCR was conducted on the same material that was sent for sequencing to validate the GROseq samples. Figure 17 shows that while there is some increase in the expression of stress genes *HSP26* and *DDR2* in the K1487R strain, it is weak and not statistically significant. This suggests that the differences between these strains may be small, and thus will require more replicates to validate with statistical confidence.

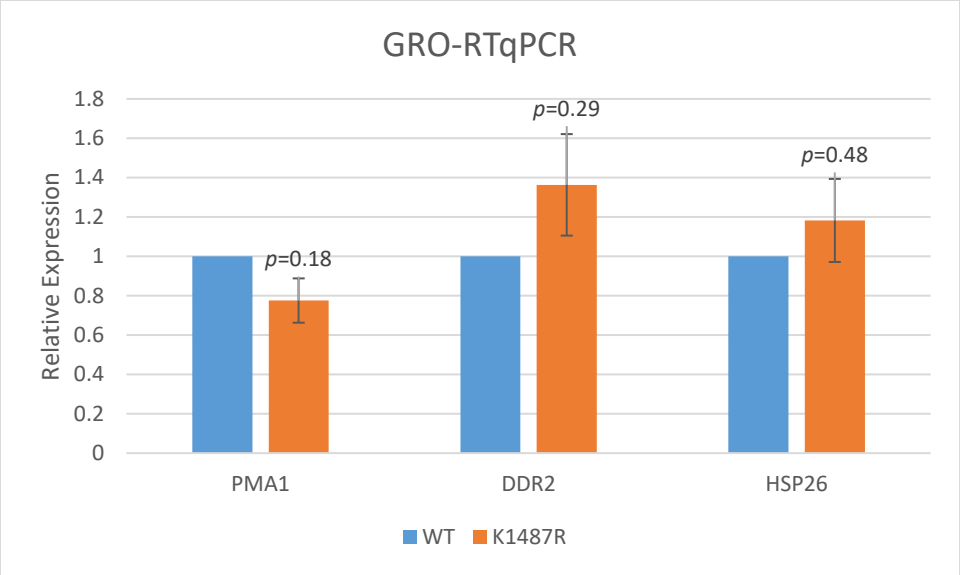

Figure 17: GRO RT-qPCR of WT and K1487R. RT-qPCR of GRO samples. Relative expression was determined by normalization to 25S rRNA, which is transcribed by RNAPI (Kuai et al., 2004). Replicates were averaged and fold changes were scaled to 1 (WT) for improved readability.

Subsequent RT-qPCR of steady state RNA was also conducted to examine any possible differences in mature mRNA levels for targets identified both in the ChIPseq and GROseq data. Figure 18 shows that, with the exception of a quite small, though statistically significant decrease for *HSP26* mRNA in K1487R, there are virtually no differences in transcription between WT and K1487R strains. This perhaps suggests that any differences in the K1487R mutant occur largely during active transcriptional processes, and may be subtle enough to be compensated for by other mRNA regulatory processes.

Figure 18: RT-qPCR of WT and K1487R RNA. 3 replicates were analyzed for each WT and K1487R strain. Fold enrichment was determined by normalization to 25S rRNA. Replicates were averaged and fold changes were scaled to 1 (WT) for improved readability.

3.3.6 RNAPII binding is unaffected by the K1487R mutation during normal growth

To complement the GROseq results described above, RNAPII ChIPseq was also performed in the WT and K1487R strains during normal growth. RNAPII ChIPseq is a useful complement assay given that GROseq and RNAPII occupancy rates can both be understood to generally approximate active transcription levels (Tan & Wong, 2019). Rather than enriching nascent transcripts, as in GROseq, ChIPseq examines the occupancy of DNA-bound proteins. As with GROseq, the material is sequenced by High Throughput Sequencing (HTS) and analyzed for genome-wide differential analysis of RNAPII-binding. In this experiment, ChIPseq was performed in WT and K1487R strains during normal growth, and a differential analysis was performed for two biological replicates. Our analysis showed 982 peaks that were identified as differentially bound compared to WT, all of which showed reduced RNAPII occupancy in the K1487R mutant, and spanned a range of biological processes (Figure 19A; Supplemental Data - Figure S3).

Unfortunately, when ChIP-qPCR was performed on the material that was sent for sequencing, the results did not validate the ChIPseq results (a more detailed ChIPseq analysis can be found in Supplemental Data). Figure 19B shows that the stress genes *HSP26* and *CTT1*, as well as the ribosomal protein gene *RPL25*, all showed an increase in RNAPII occupancy in the K1487R strain when measured by ChIP-qPCR, contradicting the ChIPseq results. While the constitutively expressed *PMA1* showed reduced RNAPII occupancy in the K1487R mutant in both ChIPseq and ChIP-qPCR analyses, the overall inconsistency in agreement between methods limits our ability to make valid conclusions about the ChIPseq dataset at this time.

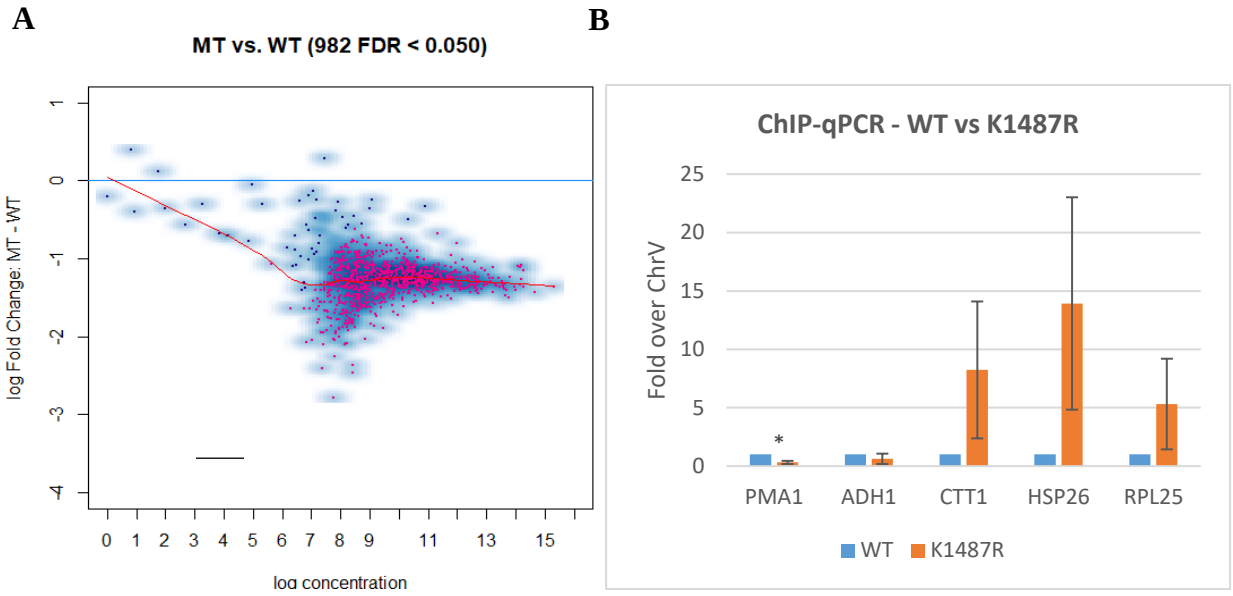

Figure 19: Differential binding analysis and validation for WT vs K1487R. (A) Scatterplot displaying differentially bound sites in the K1487R strain (MT), as compared to WT (significantly differentially bound shown in red) for ChIPseq data. This is a "smoothed" plot, meaning darker blue regions represent many peaks in that region, where lighter colors indicate few or no peaks. Fold change (log2) is plotted against normalized read density (log2). The red line represents a non-linear regression fit (loess) to visualize the relationship between fold change and peak intensity. **(B) ChIP-qPCR of ChIPseq samples**. Two replicates were analyzed for each WT and K1487R strain. Fold-enrichment was determined by normalization to ChrV (non-transcribed region). Replicates were averaged and fold changes were scaled to 1 (WT) for improved readability.

Section 4: Discussion and Next Steps

The results presented in Section 3 detail several important findings. They show that chromatin-associated Rpb1 is more likely to be sumoylated than soluble Rpb1, that Rpb1 sumoylation is rapidly deconjugated by Ulp1, and that the unexpectedly low levels of sumoylated Rpb1 observed in the absence of the SUMO protease Ulp2 does not appear to involve ubiquitin- and proteasome-mediated degradation. Regarding the major sumoylation site of Rpb1, K1487, while mutating this conjugation site impairs Rpb1 sumoylation, there appears to be no impact on growth under non-stressed conditions, or on the interaction of Rpb1 with the nucleosome remodeler Spt6. Interestingly, genome-wide nascent transcription analysis shows that a small subset of genes are modestly upregulated in the K1487R mutant during normal growth, though more replicates are required to provide statistical confidence. In this section, several of these findings are discussed in an effort to offer possible explanations for the observed outcomes and to outline next steps that may further these objectives.

4.1 Role of Ulp2 in regulating sumoylated Rpb1 remains unclear

As Section 3.2 establishes that reduced levels of sumoylated Rpb1 in the *ulp2Δ* mutant does not appear to be due to proteasome-mediated degradation, the reason for this finding remains unclear. One possible explanation is that, because of a global reduction in desumoylation that occurs in this mutant, perhaps there is an associated shortage of free SUMO available for Rpb1. That is, perhaps the pool of normally available free SUMO is instead attached to other conjugates and unavailable for Rpb1 conjugation. An experiment to measure this could involve providing the cell with ample SUMO (by overexpressing SUMO using an integrated plasmid) in a *ulp2Δ* background. Should such a test show a relative increase in Rpb1 sumoylation, this would provide a plausible explanation as to why reduced Rpb1 sumoylation

was observed in a *ulp2Δ* strain. However, because it has been shown that high expression of mature SUMO in a *ulp2Δ* background in fact impairs growth (Schwienhorst et al., 2000), any observed rescue of sumoylated Rpb1 levels should be assessed in the context of overall cell fitness.

Another possibility is that reduced Rpb1 sumoylation in the *ulp2Δ* is merely a product of the large-scale transcriptional downregulation that has been observed in this mutant (Ryu et al., 2019). Indeed, it has been shown that Ulp2 plays an important role in transcriptional activation, facilitating RNAPII elongation and showing an overall reduction in RNAPII occupancy at transcriptionally active sites in the *ulp2Δ* mutant (Ryu et al., 2019). Consider also that reduced Rpb1 sumoylation in the *ulp2Δ* mutant is accompanied by relatively unchanged global levels of Rpb1 (Figure 8B), and, as was shown in Figure 5A, a greater proportion of chromatin-associated Rpb1 is sumoylated than soluble Rpb1. Taken together, it stands to reason that the level of sumoylated Rpb1 may be closely tied with transcriptionally activity. This could be further examined by conducting a chromatin fractionation in WT and *ulp2Δ* strains to see if the amount of chromatin-associated Rpb1 indeed decreases in the *ulp2Δ* strain, as would be expected under this hypothesis.

It would also be interesting to contrast the ratio of sumoylated-Rpb1 to total Rpb1 between WT and *ulp2Δ*, specifically within the chromatin-associated fraction of lysate. This would largely exclude soluble Rpb1 from the analysis, and thus allow a more meaningful interpretation of the role sumoylated-Rpb1 plays in transcriptional processes. To do this, an Rpb1-IP would be performed on the chromatin-associated fraction of WT and *ulp2Δ* material, immunoblotted for SUMO and Rpb1 (as was done for WT cells in Figure 5A).

4.2 Sumoylated Rpb1 may negatively regulate genes associated with the stress response during non-stressed growth

As previously mentioned, the first steps in furthering the work described in Section 3.3.4 involves repeating the GROseq experiment with additional replicates. Because the findings suggest the effects are small, more replicates would provide additional statistical confidence. Nevertheless, the finding that the SUMO-compromised Rpb1 is associated with an increase in nascent transcripts of several stress genes is an interesting finding and suggests that this modification may be important for negatively regulating these genes during normal growth. Indeed, Moallem et al. (2023) reported that the fraction of protein-coding genes (in *S. cerevisiae*) that show changes in RNAPII occupancy during heat shock increases from ~6% to ~30% when global levels of sumoylation are reduced. Recalling that GROseq and RNAPII occupancy rates can be understood to generally approximate active transcription levels (Tan & Wong, 2019), this suggests that sumoylation, generally speaking, may play a role in tempering transcriptional changes during heat shock (Moallem et al., 2023). While this GROseq experiment examined only a single sumoylation-impaired transcriptional element (Rpb1) under non-stressed conditions, perhaps there is a shared mechanism by which sumoylation provides a check on inappropriate transcriptional behavior.

Though it is unclear how sumoylated Rpb1 may accomplish this selective transcriptional repression, one possibility may involve regulating mRNA stability. One example of this has been reported in the literature for the sumoylated transcription factor Rap1, which has been suggested to regulate the expression of some ribosomal protein genes both positively and negatively: positively, by facilitating transcription activator binding, but also negatively by tempering expression by facilitating mRNA degradation (Chymkowitch et al., 2015). Should a similar process be occurring with Rpb1, it could be consistent with the observed upregulated stress

genes in the GROseq results, as there is perhaps exceptional pressure to restrain expression levels under normal growth conditions. In other words, if sumoylated Rpb1 is involved with negatively regulating mRNA levels, it would be expected that impairing Rpb1-sumoylation could lead to an increase in observed nascent transcripts of stress genes. Further research that focuses on the ability of the K1487R strain to manage transcription during stress conditions, as well as examining mRNA stability, would allow for careful scrutiny of these hypotheses. Further details regarding specific next steps are discussed below in Section 4.4.

4.3 Rpb1-K1487R may reduce overall RNAPII occupancy, but additional efforts are required to validate

The source of disagreement between ChIPseq and ChIP-qPCR for the analysis in Section 3.3.6 is unclear. But it is important to note that while ChIP-qPCR is a standard method of ChIPseq validation, ChIP-qPCR and ChIPseq each have unique areas of potential bias that could complicate validation when differences are not dramatic. One such possibility involves how peaks are measured: whereas ChIPseq identifies and compares peak regions as determined by peak-calling software, ChIP-qPCR measures only a specific region as determined by primer homology. While the primers used for this study do target regions of downregulated K1487R read coverage (as determined by visual inspection of aligned sequence file coverage), targeting multiple regions of this gene would provide a more robust validation of *RPL25* by qPCR. Furthermore, thorough validation of each primer set through the use of a standard curve for efficiency assessment, coupled with a melt curve to detect off-target effects, can significantly help in identifying potential PCR-related biases.

It is also important to note that ChIP-qPCR data are normalized differently from ChIPseq data. Whereas ChIPseq analysis uses the local background read coverage to normalize peaks, our

ChIP-qPCR method uses an untranscribed region of chromosome V as a normalizing target, as it represents signal that can be attributed to non-specific binding during the IP. This is a standard practice that makes practical sense, since targeting numerous background regions to gain a better estimation of the general background can be an unnecessarily onerous task when conducting a qPCR-based assay. But because this one target serves as a proxy for the overall background level - where small differences can greatly affect fold-enrichment - there is greater risk of variable results between replicates. One strategy currently being developed to address this involves the implementation of a positive control, whereby a well-established and high-occupancy DNA-binding protein is targeted by a second antibody. Such a system should prove more robust to varying background levels, which would only account for a small fraction of the peak intensity at this high-occupancy site.

4.4 Heat shock as a condition for studying Rpb1-sumoylation requirements

While Rpb1-K1487R has been shown repeatedly in our lab to reduce Rpb1 sumoylation, some of my experiments indicate that, while the mutation consistently changes the characteristic pattern of Rpb1 sumoylation, the overall sumoylation level does not always appear to decrease appreciably (Figure 20). And while the change in the Rpb1 sumoylation pattern itself may impact the biological behavior of Rpb1, because there is inconsistency in the degree to which Rpb1 is sumoylated between experiments, this suggests there may be certain conditions not yet accounted for in our methods that affect the overall level of Rpb1 sumoylation during normal growth (ODs at collection, different lots of media, etc.). Accordingly, further characterization of Rpb1-K1487R sumoylation during normal growth should pay careful attention to all aspects of growth conditions, such as harvesting OD, level of starting culture saturation prior to exponential growth, how recent colonies used for studies were streaked on agar plates, etc. While small

variations in these conditions do not tend to impact reproducible research in our lab, they may nevertheless be uniquely important factors that influence the level of Rpb1-sumoylation during normal growth.

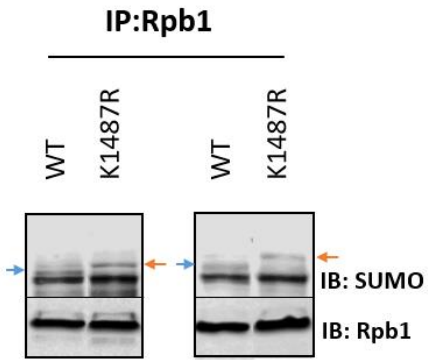

Figure 20: Rpb1 sumoylation is mostly at K1487. Western Blot of two additional Rpb1-IP replicates with arrows indicating polysumoylation bands lost (blue) and gained (orange) in the K1487R strain.

However, given recently published findings in our lab, a more fruitful approach may be one that examines the ability of the Rpb1-K1487R mutant to manage transcription during stress, and particularly during heat shock. Moallem et al. (2023) showed that normal levels of sumoylation, achieved by dynamic conjugation and deconjugation, are required for cells to achieve a characteristic increase in global SUMO conjugation that is induced with heat shock. It was further reported that whereas the expression of less than 10% of all protein-coding genes are effected during heat shock, reduced global sumoylation resulted in transcriptional changes in ~30% of all protein-coding genes (Moallem et al., 2023). This highlights the importance of a healthy sumoylation system to a stress-induced transcriptional response. It may thus be interesting to conduct a similar analysis in the K1487R strain, and examine to what degree (if any) this sumoylation-impaired Rpb1 plays a role in the heat shock-induced transcriptional response.

First steps would include identifying the optimal heat shock conditions where Rpb1 sumoylation is maximized, testing cells at 37°C, 39°C and 42°C. Once optimal conditions are identified, heat shock-induced WT and K1487R strains should be examined to determine if the K1487R mutation impacts the identified increase in Rpb1 sumoylation. If so, ChIPseq should be considered to profile any genome-wide impacts on transcription. Growth curves could also be performed to determine if post-heat shock growth is affected by the K1487R mutant.

4.5 Combining the K1487R strain with the sumoylation-impaired Tfg1-K60/61R mutation

It was previously reported that multiple elements of the heat shock protein complex formation needed to be rendered SUMO-impaired (rather than just one) in order to have a functional impact, in an effect dubbed "group sumoylation" (Psakhye & Jentsch, 2012). This is an intriguing model, and perhaps sumoylation of the PIC is an analogous context: That is, one explanation as to why the Rpb1-K1487R strain shows little or no effect on RNAPII occupancy is because the PIC is still being sufficiently sumoylated at other elements of the complex. This possibility was also considered by Baig et al. (2021) who found that a sumoylation-impaired Tfg1 (the most sumoylated subunit of TFIIF) showed reduced RNAPII occupancy across the genome during normal growth, but no associated changes in steady state mRNA levels.

With this in mind, I have generated a sumoylation-impaired Rpb1 and a sumoylation impaired Tfg1 contained in the same strain. While it may ultimately prove necessary to impair sumoylation of multiple elements of the PIC in order to have a functional impact, given that most TFIIFs are complexed with RNAPII (Rani et al., 2004), Tfg1 is a reasonable next target for reducing sumoylation at the PIC.

4.6 Examining the effect of permanently sumoylating Rpb1

Finally, building on the research by Baig et al. (2021), who developed a permanently sumoylated form of Tfg1 (SUMO-Tfg1) to examine the transcriptional effects of persistent sumoylation of this GTF, a similar approach could be considered with Rpb1. As with Tfg1, a SUMO-Rpb1 fusion mutant could provide additional useful information about sumoylation-mediated RNAPII regulation. Interestingly, the SUMO-Tfg1 fusion was reported to exhibit a number of unique effects, including reduced association with RNAPII, significantly reduced RNAPII levels at protein coding genes, and a modest growth defect at elevated temperatures (Baig et al, 2021). Examining the effect of a fusion SUMO-Rpb1 in each of these contexts could be quite useful. Specifically, it would be interesting to compare the biological effect of the SUMO-Rpb1 fusion with the SUMO-Tfg1 fusion. Because their SUMO-impaired counterparts (Rpb1-K1487R and Tfg1-K60/61R, respectively) shared some similar effects (no growth defects, potential reduction in RNAPII occupancy across the genome), it would be interesting to see if the SUMO-Rpb1 and SUMO-Tfg1 fusions also shared similar biological outcomes. If their similarities indeed extended to their fusion counterparts, the concept of "group sumoylation" could have considerable import here, and inform the direction of further study. That is, similar to the discussion in Section 4.5, perhaps the functional importance of persistent sumoylation of either element lies in excessive sumoylation of the PIC overall, rather than the discrete deficiencies of either element. To examine this possibility, a SUMO-Rpb1 fusion strain has been constructed such that the fused SUMO is located at the K1487 residue (whereas the SUMO-Tfg1 was an N-terminal fusion) to approximate the endogenous sumoylated form as much as possible (Figure 21).

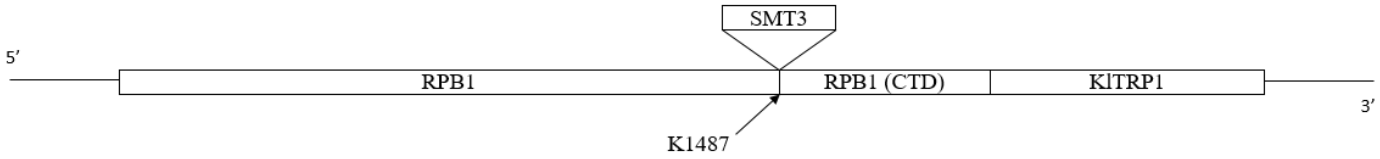

Figure 21: Schematic of Rpb1-SUMO fusion strain. Schematic of Rpb1-SUMO fusion strain design. The SUMO-encoding *SMT3* was inserted at the major sumoylation site, replacing K1487, rather than attaching SUMO at the C-terminal or N-terminal site, as is typically done for fusion proteins. The rationale here is that the flexible nature of the linker region will facilitate proper folding and function of SUMO at this location.

There are a couple of experimental advantages to placing SUMO in this location. First, persistently sumoylating K1487 could provide useful information about the Rpb1/Spt6 association (which occurs in this region) that would not be possible with an N-terminal fusion. And while the K1487R mutant did not show reduced interaction with this nucleosome remodeler (Spt6), perhaps the permanently sumoylated Rpb1 at this location will. Furthermore, preliminary immunoblots with this mutant have shown that the SUMO-Rpb1 fusion may be hyperphosphorylated at the CTD (data not shown). As such, subsequent examination of Ser2 and Ser5 phosphorylation of the CTD in this strain may provide additional insight to potential stage-specific requirements or biases for Rpb1-sumoylation during transcription.

There is an important caveat to this system: introducing SUMO in the peptide chain at this location generates an artificial gap between the residues on either side of K1487, which may impact the way SUMO typically functions at this site. However, for studying the interaction between Spt6 and SUMO-K1487, this limitation is arguably a preferable trade-off to established approaches that fuse at the N-terminal or C-terminal regions, which would not address the potential interaction of SUMO at K1487.

4.7 Conclusion

In this work presented, I have demonstrated that Rpb1 is sumoylated under normal conditions, is mostly associated with chromatin, and is subject to dynamic

conjugation/deconjugation. I have also shown that the decrease in polysumoylation of Rpb1 in a *ulp2Δ* background is unlikely to be a result of an unstable complex that is ultimately degraded. While the specific role Ulp2 plays in maintaining normal levels of Rpb1 sumoylation is still unclear, I have outlined strategies for examining the extent to which Rpb1 can be polysumoylated in a *ulp2Δ* background. I also show that the sumoylation-impaired Rpb1-K1487R is associated with an increase in nascent transcription for roughly two dozen genes, more than a quarter of which are associated with the stress response. Interestingly, further characterizations reveal that a sumoylation-impaired Rpb1 does not appear to impact normal growth, steady state RNA levels, or the association of Rpb1 with the transcriptional activator Spt6. Taking into account findings from recently published work in our lab regarding global sumoylation requirements for heat shock in our lab, next steps should focus on specifically examining Rpb1-sumoylation requirements for managing heat shock. Combing the sumoylation-impaired Rpb1 with the sumoylation-impaired Tfg1 may also yield useful insights into sumoylation requirements of the PIC more generally.

Appendix: Supplementary Data: RNAPII ChIPseq analysis

The ChIP assay involves fixing cells such that chromatin-bound proteins are crosslinked to DNA. The chromatin is then fragmented (in this case by sonication) and solubilized to facilitate enrichment for a protein-linked DNA target of interest (in this case, RNAPII) through immunoprecipitation. Fragments of DNA bound by this protein are then purified and typically analyzed by qPCR or high-throughput sequencing (HTS) to examine target protein occupancy (see Section 2.6 and Table 4 for additional details).

In this experiment, ChIPseq was performed on three biological replicates for each strain. Because initial clustering of sample data showed poor correlation of K1487R replicate 3 (Figure S1) with its associated replicates, replicate 3 was subsequently removed from the dataset prior to further analysis.

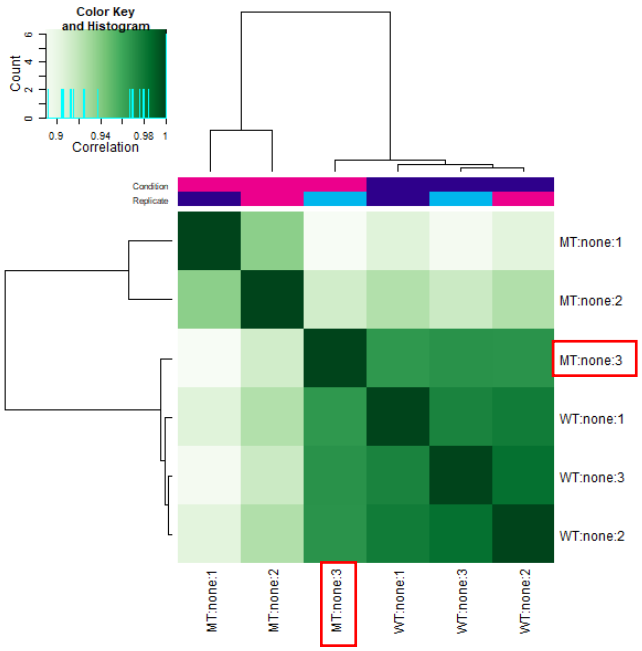

Figure S1: Quality control of ChIPseq raw data. A clustering heatmap that was generated to analyze correlation between each sample across the binding matrix (at each peak). Increased correlation is indicated by darker squares on the heatmap. K1487R replicate 3 (outlined in red "MT:none:3") appears to correlate better with WT samples than its associated replicates.

As described in Section 3.3.6, 982 peaks were identified as differentially bound in the K1487R mutant, all of which showed reduced RNAPII occupancy. Figure S2 shows examples of coverage profiles generated in IGV for the constitutively expressed gene *PMA1* and the ribosomal protein gene *RPL25*, both of which were identified as differentially bound (reduced) in the K1487R mutant. It also shows the stress gene *HSP26*, which was not identified as differentially bound in this analysis.

To probe the biological relevance of these differences, we next examined biological processes that may be overrepresented by the genes associated with the differential peakset (genes associated with peaks that were identified as differentially bound in K1487R mutant). To do this, a gene ontology (GO) term analysis was performed. This analysis revealed many biological processes to be overrepresented, with genes associated with cytoplasmic translation displaying the greatest fold-change and level of significance among those processes (Figure S3).

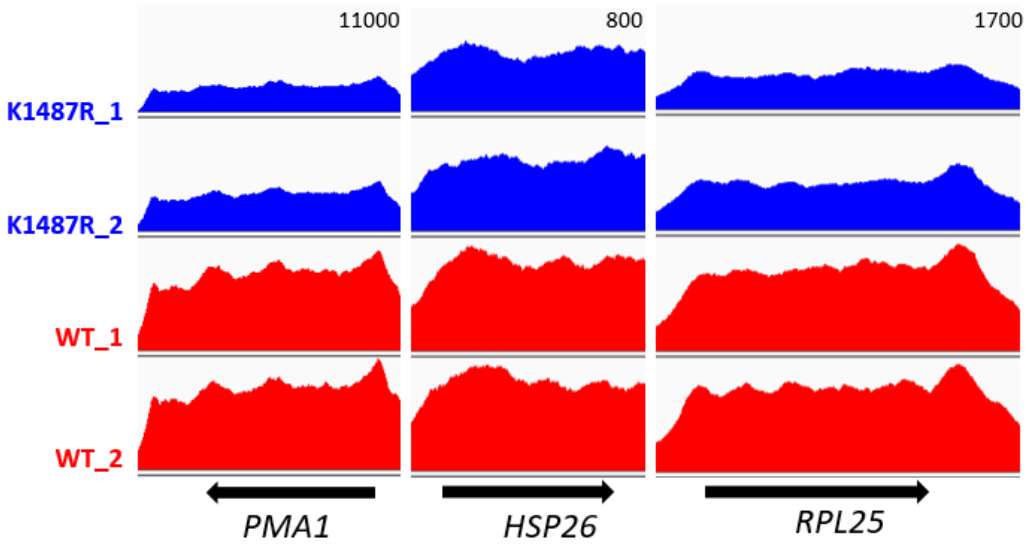

Figure S2: Read coverage alignments for select genes: Unnormalized read coverage alignments for RNAPII-ChIPseq in WT and K1487R samples for constitutively expressed gene *PMA1*, the ribosomal protein gene *RPL25*, and the heat shock gene *HSP26*. *PMA1* and *RPL25* were identified as differentially expressed, but *HSP26* was not. Images for all genes were generated in IGV. Numbers in the top right corner of each alignment indicate range of read coverage.

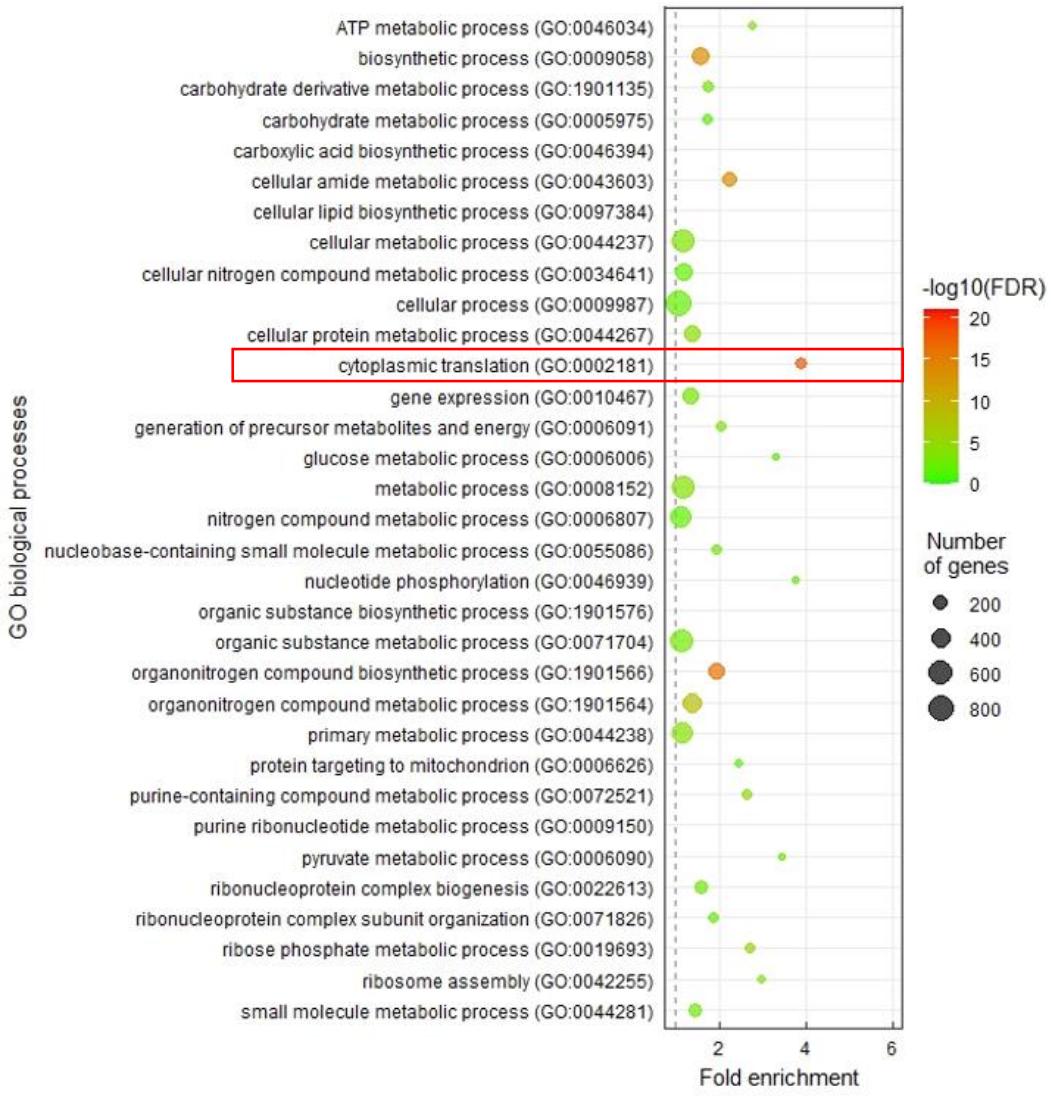

Figure S3: WT vs K1487 Gene Ontology analysis. GO term analysis of the genes associated with differentially bound sites. Biological processes that are overrepresented in the K1487R strain are identified. Fold enrichment refers to the degree to which the process is overrepresented within the set of genes associated with differentially bound sites.

Interestingly, cytoplasmic translation was also identified as the most elevated process in a previous ChIPseq experiment that was completed in our lab that examined RNAPII levels in a *ubc9-6* strain, where global sumoylation levels are reduced due to a point mutation in the sole E2

conjugating enzyme Ubc9 (Moallem et al., 2023). Surprisingly, however, genes associated with cytoplasmic translation were upregulated in the *ubc9-6* strain (as compared to its WT), whereas they were downregulated in this analysis. It is unclear (but interesting) why altering Rpb1-sumoylation only (as in the K1487R mutant) would have near-opposite and dramatic effects on this particular subset of genes, as compared to a cellular environment where global sumoylation is reduced (as in the *ubc9-6* mutant). But as sumoylation is implicated in a myriad of processes, it is conceivable that reducing global sumoylation could cause a number of knock-on effects that ultimately influence RNAPII binding at genes involved in cytoplasmic translation in unexpected ways.

References

Al-Husini, N., Sharifi, A., Mousavi, S. A., Chitsaz, H., & Ansari, A. (2017). Genomewide Analysis of Clp1 Function in Transcription in Budding Yeast. *Scientific reports*, *7*(1), 6894. https://doi.org/10.1038/s41598-017-07062-6

Alquezar, C., Arya, S., & Kao, A. W. (2021). Tau Post-translational Modifications: Dynamic Transformers of Tau Function, Degradation, and Aggregation. *Frontiers in neurology*, *11*, 595532. https://doi.org/10.3389/fneur.2020.595532

Bilsland, E., Molin, C., Swaminathan, S., Ramne, A., & Sunnerhagen, P. (2004). Rck1 and Rck2 MAPKAP kinases and the HOG pathway are required for oxidative stress resistance. *Molecular microbiology*, *53*(6), 1743–1756. https://doi.org/10.1111/j.1365-2958.2004.04238.x

Baig, M. S., Dou, Y., Bergey, B. G., Bahar, R., Burgener, J. M., Moallem, M., McNeil, J. B., Akhter, A., Burke, G. L., Sri Theivakadadcham, V. S., Richard, P., D'Amours, D., & Rosonina, E. (2021). Dynamic sumoylation of promoter-bound general transcription factors facilitates transcription by RNA polymerase II. *PLoS genetics*, *17*(9), e1009828. https://doi.org/10.1371/journal.pgen.1009828

Bylebyl, G. R., Belichenko, I., & Johnson, E. S. (2003). The SUMO isopeptidase Ulp2 prevents accumulation of SUMO chains in yeast. *The Journal of biological chemistry*, *278*(45), 44113–44120. https://doi.org/10.1074/jbc.M308357200

Celen, A. B., & Sahin, U. (2020). Sumoylation on its 25th anniversary: mechanisms, pathology, and emerging concepts. *The FEBS journal*, *287*(15), 3110–3140. https://doi.org/10.1111/febs.15319

Chang YC, Oram MK, Bielinsky AK. SUMO-Targeted Ubiquitin Ligases and Their Functions in Maintaining Genome Stability. Int J Mol Sci. (2021) May 20;22(10):5391. doi: 10.3390/ijms22105391. PMID: 34065507; PMCID: PMC8161396.

Chen, X., Ding, B., LeJeune, D., Ruggiero, C., & Li, S. (2009). Rpb1 sumoylation in response to UV radiation or transcriptional impairment in yeast. *PloS one*, *4*(4), e5267.https://doi.org/10.1371/journal.pone.0005267

Chymkowitch, P., Nguéa, A. P., Aanes, H., Koehler, C. J., Thiede, B., Lorenz, S., Meza-Zepeda, L. A., Klungland, A., & Enserink, J. M. (2015). Sumoylation of Rap1 mediates the recruitment of TFIID to promote transcription of ribosomal protein genes. Genome research, 25(6), 897–906. https://doi.org/10.1101/gr.185793.114

Chun, Y., Joo, Y. J., Suh, H., Batot, G., Hill, C. P., Formosa, T., & Buratowski, S. (2019). Selective Kinase Inhibition Shows That Bur1 (Cdk9) Phosphorylates the Rpb1 Linker *In Vivo*. *Molecular and cellular biology*, *39*(15), e00602-18. https://doi.org/10.1128/MCB.00602-18

Cramer, P., Bushnell, D. A., & Kornberg, R. D. (2001). Structural basis of transcription: RNA polymerase II at 2.8 angstrom resolution. *Science (New York, N.Y.)*, *292*(5523), 1863–1876. https://doi.org/10.1126/science.1059493

Cramer, P., Armache, K. J., Baumli, S., Benkert, S., Brueckner, F., Buchen, C., Damsma, G. E., Dengl, S., Geiger, S. R., Jasiak, A. J., Jawhari, A., Jennebach, S., Kamenski, T., Kettenberger, H., Kuhn, C. D., Lehmann, E., Leike, K., Sydow, J. F., & Vannini, A. (2008). Structure of eukaryotic RNA polymerases. *Annual review of biophysics*, *37*, 337–352. https://doi.org/10.1146/annurev.biophys.37.032807.130008

Cremona, C. A., Sarangi, P., & Zhao, X. (2012). Sumoylation and the DNA damage response. *Biomolecules*, *2*(3), 376–388. https://doi.org/10.3390/biom2030376

Cuevas-Bermúdez, A., Garrido-Godino, A. I., & Navarro, F. (2019). A novel yeast chromatin-enriched fractions purification approach, yChEFs, for the chromatin-associated protein analysis used for chromatin-associated and RNA-dependent chromatin-associated proteome studies from Saccharomyces cerevisiae. *Gene Reports*, *16*, 100450.

Eckhoff, J., & Dohmen, R. J. (2015). In Vitro Studies Reveal a Sequential Mode of Chain Processing by the Yeast SUMO (Small Ubiquitin-related Modifier)-specific Protease Ulp2. *The Journal of biological chemistry*, *290*(19), 12268–12281. https://doi.org/10.1074/jbc.M114.622217

Gasch, A. P., Spellman, P. T., Kao, C. M., Carmel-Harel, O., Eisen, M. B., Storz, G., Botstein, D., & Brown, P. O. (2000). Genomic expression programs in the response of yeast cells to environmental changes. *Molecular biology of the cell*, *11*(12), 4241–4257. https://doi.org/10.1091/mbc.11.12.4241

Harlen, K. M., & Churchman, L. S. (2017). The code and beyond: transcription regulation by the RNA polymerase II carboxy-terminal domain. *Nature reviews. Molecular cell biology*, *18*(4), 263–273. https://doi.org/10.1038/nrm.2017.10

Hauser, M., Abraham, P. E., Barcelona, L., & Becker, J. M. (2019). UV Laser-Induced, Time-Resolved Transcriptome Responses of *Saccharomyces cerevisiae*. *G3 (Bethesda, Md.)*, *9*(8), 2549–2560. https://doi.org/10.1534/g3.119.400291

Hay R. T. (2006). Role of ubiquitin-like proteins in transcriptional regulation. *Ernst Schering Research Foundation workshop*, (57), 173–192. https://doi.org/10.1007/3-540-37633-x_10

Heckmann, I., Kern, M. J., Pfander, B., & Jentsch, S. (2019). A SUMO-dependent pathway controls elongating RNA Polymerase II upon UV-induced damage. *Scientific reports*, *9*(1), 17914. https://doi.org/10.1038/s41598-019-54027-y

Hendriks, I. A., & Vertegaal, A. C. (2016). A comprehensive compilation of SUMO proteomics. *Nature reviews. Molecular cell biology*, *17*(9), 581–595. https://doi.org/10.1038/nrm.2016.81

Hickey, C. M., Wilson, N. R., & Hochstrasser, M. (2012). Function and regulation of SUMO proteases. Nature reviews. *Molecular cell biology*, *13*(12), 755–766. https://doi.org/10.1038/nrm3478

Kisselev, A. F., van der Linden, W. A., & Overkleeft, H. S. (2012). Proteasome inhibitors: an expanding army attacking a unique target. *Chemistry & biology*, *19*(1), 99–115. https://doi.org/10.1016/j.chembiol.2012.01.003

Knop, M., Siegers, K., Pereira, G., Zachariae, W., Winsor, B., Nasmyth, K., & Schiebel, E. (1999). Epitope tagging of yeast genes using a PCR-based strategy: more tags and improved practical routines. *Yeast (Chichester, England)*, *15*(10B), 963–972. https://doi.org/10.1002/(SICI)1097-0061(199907)15:10B<963::AID-YEA399>3.0.CO;2-W

Kobayashi, N., & McEntee, K. (1990). Evidence for a heat shock transcription factor-independent mechanism for heat shock induction of transcription in Saccharomyces cerevisiae. *Proceedings of the National Academy of Sciences of the United States of America*, *87*(17), 6550–6554. https://doi.org/10.1073/pnas.87.17.6550

Kuai, L., Fang, F., Butler, J. S., & Sherman, F. (2004). Polyadenylation of rRNA in Saccharomyces cerevisiae. *Proceedings of the National Academy of Sciences of the United States of America*, *101*(23), 8581–8586. https://doi.org/10.1073/pnas.0402888101

Lee, D. H., & Goldberg, A. L. (1998). Proteasome inhibitors: valuable new tools for cell biologists. *Trends in cell biology*, *8*(10), 397–403. https://doi.org/10.1016/s0962-8924(98)01346-4

Li, S. J., & Hochstrasser, M. (2000). The yeast ULP2 (SMT4) gene encodes a novel protease specific for the ubiquitin-like Smt3 protein. *Molecular and cellular biology*, *20*(7), 2367–2377. https://doi.org/10.1128/MCB.20.7.2367-2377.2000

Matunis, M. J., Wu, J., & Blobel, G. (1998). SUMO-1 modification and its role in targeting the Ran GTPase-activating protein, RanGAP1, to the nuclear pore complex. *The Journal of cell biology*, *140*(3), 499–509. https://doi.org/10.1083/jcb.140.3.499

McNeil, J. B., Lee, S. K., Oliinyk, A., Raina, S., Garg, J., Moallem, M., Urquhart-Cox, V. Fillingham, J., Cheung, P., & Rosonina, E. (2024). 1,10-phenanthroline inhibits sumoylation and reveals that yeast SUMO modifications are highly transient. *EMBO reports*, 1-14. https://www.embopress.org/doi/abs/10.1038/s44319-023-00010-8

Moallem, M., Akhter, A., Burke, G. L., Babu, J., Bergey, B. G., McNeil, J. B., Baig, M. S., & Rosonina, E. (2023). Sumoylation is Largely Dispensable for Normal Growth but Facilitates Heat Tolerance in Yeast. *Molecular and cellular biology*, *43*(1), 64–84. https://doi.org/10.1080/10985549.2023.2166320

Muniz, L., Nicolas, E., & Trouche, D. (2021). RNA polymerase II speed: a key player in controlling and adapting transcriptome composition. *The EMBO journal*, *40*(15), e105740. https://doi.org/10.15252/embj.2020105740

Nam K. H. (2021). Structural analysis of metal chelation of the metalloproteinase thermolysin by 1,10-phenanthroline. *Journal of inorganic biochemistry*, *215*, 111319. https://doi.org/10.1016/j.jinorgbio.2020.111319

Osman, S., & Cramer, P. (2020). Structural Biology of RNA Polymerase II Transcription: 20 Years On. *Annual review of cell and developmental biology*, *36*, 1–34. https://doi.org/10.1146/annurev-cellbio-042020-021954

O'Brien, M. J., Gurdziel, K., & Ansari, A. (2023). Global Run-On sequencing to measure nascent transcription in Saccharomyces cerevisiae. *Methods (San Diego, Calif.)*, *217*, 18–26. https://doi.org/10.1016/j.ymeth.2023.06.009

Pabst, S., Döring, L. M., Petreska, N., & Dohmen, R. J. (2019). Methods to study SUMO dynamics in yeast. *Methods in enzymology*, *618*, 187–210. https://doi.org/10.1016/bs.mie.2018.12.026

Psakhye, I., & Jentsch, S. (2012). Protein group modification and synergy in the SUMO pathway as exemplified in DNA repair. Cell, 151(4), 807–820. https://doi.org/10.1016/j.cell.2012.10.021

Psakhye, I., Castellucci, F., & Branzei, D. (2019). SUMO-Chain-Regulated Proteasomal Degradation Timing Exemplified in DNA Replication Initiation. *Molecular cell*, *76*(4), 632–645.e6. https://doi.org/10.1016/j.molcel.2019.08.003

Rani, P. G., Ranish, J. A., & Hahn, S. (2004). RNA polymerase II (Pol II)-TFIIF and Pol II-mediator complexes: the major stable Pol II complexes and their activity in transcription initiation and reinitiation. *Molecular and cellular biology*, *24*(4), 1709–1720. https://doi.org/10.1128/MCB.24.4.1709-1720.2004

Ritchie, M. E., Phipson, B., Wu, D., Hu, Y., Law, C. W., Shi, W., & Smyth, G. K. (2015). limma powers differential expression analyses for RNA-sequencing and microarray studies. *Nucleic acids research*, *43*(7), e47. https://doi.org/10.1093/nar/gkv007

Rosonina E. (2019). A conserved role for transcription factor sumoylation in binding-site selection. *Current genetics*, *65*(6), 1307–1312. https://doi.org/10.1007/s00294-019-00992-w

Rosonina, E., Duncan, S. M., & Manley, J. L. (2010). SUMO functions in constitutive transcription and during activation of inducible genes in yeast. *Genes & development*, *24*(12), 1242–1252. https://doi.org/10.1101/gad.1917910

Ryu, H. Y., Su, D., Wilson-Eisele, N. R., Zhao, D., López-Giráldez, F., & Hochstrasser, M. (2019). The Ulp2 SUMO protease promotes transcription elongation through regulation of histone sumoylation. *The EMBO journal*, *38*(16), e102003. https://doi.org/10.15252/embj.2019102003

Ryu, H. Y., Wilson, N. R., Mehta, S., Hwang, S. S., & Hochstrasser, M. (2016). Loss of the SUMO protease Ulp2 triggers a specific multichromosome aneuploidy. *Genes & development*, *30*(16), 1881–1894. https://doi.org/10.1101/gad.282194.116

Sancar A. (2016). Mechanisms of DNA Repair by Photolyase and Excision Nuclease (Nobel Lecture). *Angewandte Chemie (International ed. in English)*, *55*(30), 8502–8527. https://doi.org/10.1002/anie.201601524

Schwienhorst, I., Johnson, E. S., & Dohmen, R. J. (2000). SUMO conjugation and deconjugation. *Molecular & general genetics : MGG*, *263*(5), 771–786. https://doi.org/10.1007/s004380000254

Sdano, M. A., Fulcher, J. M., Palani, S., Chandrasekharan, M. B., Parnell, T. J., Whitby, F. G., Formosa, T., & Hill, C. P. (2017). A novel SH2 recognition mechanism recruits Spt6 to the doubly phosphorylated RNA polymerase II linker at sites of transcription. eLife, 6, e28723. https://doi.org/10.7554/eLife.28723

Suh, H., Hazelbaker, D. Z., Soares, L. M., & Buratowski, S. (2013). The C-terminal domain of Rpb1 functions on other RNA polymerase II subunits. *Molecular cell*, *51*(6), 850–858. https://doi.org/10.1016/j.molcel.2013.08.015

Tan, K., & Wong, K. H. (2019). RNA polymerase II ChIP-seq-a powerful and highly affordable method for studying fungal genomics and physiology. Biophysical reviews, 11(1), 79–82. https://doi.org/10.1007/s12551-018-00497-9

Tatham, M. H., Jaffray, E., Vaughan, O. A., Desterro, J. M., Botting, C. H., Naismith, J. H., & Hay, R. T. (2001). Polymeric chains of SUMO-2 and SUMO-3 are conjugated to protein substrates by SAE1/SAE2 and Ubc9. *The Journal of biological chemistry*, *276*(38), 35368–35374. https://doi.org/10.1074/jbc.M104214200

Travas. A. (2021). *The Rpb1 subunit of transcriptionally active RNA Polymerase II is sumoylated in normal growth conditions* [unpublished undergraduate's thesis]. York University.

Tristan, C., Shahani, N., Sedlak, T. W., & Sawa, A. (2011). The diverse functions of GAPDH: views from different subcellular compartments. Cellular signalling, 23(2), 317–323. https://doi.org/10.1016/j.cellsig.2010.08.003

Uzunova, K., Göttsche, K., Miteva, M., Weisshaar, S. R., Glanemann, C., Schnellhardt, M., Niessen, M., Scheel, H., Hofmann, K., Johnson, E. S., Praefcke, G. J., & Dohmen, R. J. (2007). Ubiquitin-dependent proteolytic control of SUMO conjugates. *The Journal of biological chemistry*, *282*(47), 34167–34175. https://doi.org/10.1074/jbc.M706505200

Vertegaal A. C. O. (2022). Signalling mechanisms and cellular functions of SUMO. Nature reviews. Molecular cell biology, 23(11), 715–731. https://doi.org/10.1038/s41580-022-00500-y

Vos, S. M., Farnung, L., Boehning, M., Wigge, C., Linden, A., Urlaub, H., & Cramer, P. (2018). Structure of activated transcription complex Pol II-DSIF-PAF-SPT6. *Nature*, *560*(7720), 607–612. https://doi.org/10.1038/s41586-018-0440-4

Wang, Q., Xue, H., Li, S., Chen, Y., Tian, X., Xu, X., Xiao, W., & Fu, Y. V. (2017). A method for labeling proteins with tags at the native genomic loci in budding yeast. *PloS one*, *12*(5), e0176184. https://doi.org/10.1371/journal.pone.0176184

Watson, J. D., Baker, T. A., Bell, S. P., Gann, A., Levine, M., Losick, R. (2004). *Molecular Biology of the Gene*. (5th ed.). Pearson.

Wild, T., & Cramer, P. (2012). Biogenesis of multisubunit RNA polymerases. *Trends in biochemical sciences*, *37*(3), 99–105. https://doi.org/10.1016/j.tibs.2011.12.001

Zeng C, Kim E, Warren SL, Berget SM. Dynamic relocation of transcription and splicing factors dependent upon transcriptional activity. EMBO J. 1997 Mar 17;16(6):1401-12. doi: 10.1093/emboj/16.6.1401. PMID: 9135155; PMCID: PMC1169737.

Table 1: List of *S. cerevisiae* strains used in these studies

Name	Lab Code	Genotype	Source
W303a	YER058	*MAT a ura3-52 trp1Δ2 leu2-3_112 his3-11 ade2-1 can1-100*	Dharmacon
RPB1	YMS001A	*RPB1::KanMX*	Mostafa Sedky
rpb1-K1487R	YMS002B	*rpb1-K1487R::KanMX*	Mostafa Sedky
ULP1	ERYM487	*leu2-3,112 ura3-52 trp1-289 ade2Δ ade3Δ lys1::kanMX4*	Emanuel Rosonina (from Maritine Heude)
ulp1-I615N (ulp1-mt)	ERYM486	*ulp1-I615N leu2-3,112 ura3-52 trp1-289 ade2Δ ade3Δ lys1::kanMX4*	Emanuel Rosonina (from Maritine Heude)
ulp2Δ	ERYM579	*ulp2Δ::URA3MX*	Emanuel Rosonina
slx5Δ	ERYM484	*slx5Δ::KanMX*	Emanuel Rosonina
ulp2Δ slx5Δ	YBB060A	*ulp2Δ::URA3 slx5Δ::KanMX*	This study
SPT6-6HA RPB1-WT::kanMX	YBB065A	*SPT6-6HA::Kl TRP1 RPB1::KanMX*	This study
SPT6-6HA rpb1-K1487R	YBB066A	*SPT6-6HA::Kl TRP1 rpb1-K1487R::KanMX*	This study
sub1-Y66A-6HA	YBB002A	*sub1-Y66A-6HA::KlTRP1*	Benjamin Bergey

Table 2: Sequence of primers used in this study

Gene	Region	Use Case	Direction	Sequence (5' to 3')
ChrV	Untranscribed	ChIP	F	CATTATCCGTAACGCCACTTT
			R	CGATCTTAGTTCCAATGGTGAAA
ADH1	Promoter	ChIP	F	GTTTGCTGTCTTGCTATCAA
			R	GAAAAAGAAACAAGGAAGAA
PMA1	Promoter	ChIP	F	CAATTATGACCGGTGACGAAAC
			R	AATCGAAACTAATGGAGGGGAG
CTT1	ORF	ChIP/RT-qPCR	F	GGCTCCCACCCTGATTATAATC
			R	GTTCGGGTGTCATTGTTTGCAC
HSP26	ORF	ChIP/GROqPCR /RT-qPCR	F	TACTGGCAAGGAAGTTGCTAG
			R	TCATCTAAGGTTTCATCTCTGG
DDR2	ORF	GROqPCR/RT-qPCR	F	TTCATTTCTGCCATCTCTGTC
			R	GTTACTCGTGGTGTTGGATG
PMA1	ORF	GROqPCR	F	CTGGTCCATTCTGGTCTTCTATC
			R	TCAGACCACCAACCGAATAAG
25S	ORF	GROqPCR RT-qPCR	F	TCTAGCATTCAAGGTCCCATTC
			R	CCCTTAGGACATCTGCGTTATC
ADH1	ORF	RT-qPCR	F	CACCGTTTTGGTCGGTATGC
			R	GACCAAACCTCTGGCGAAGA
RPS27B	ORF	RT-qPCR	F	ATGTCAAATGCCCAGGTTGT
			R	TGACAGCAGTTTGAGCATGA
RPL25	ORF (intron)	RT-qPCR	F	ACCAACAGCCATTAACAAATCC
			R	TTAACGACAGCTTTCTTAGCG
RPL25	ORF	RT-qPCR/ChIP	F	CTATGAAGAAGGTTGAAGATGG
			R	TGGTCTAACCAAAGTGTTAACC
RPS27B	ORF (intron)	RT-qPCR	F	CTGGGTAATGATTTATCCTTC
			R	TGGGTGCAACAAATCTTGAAC
KlTRP1	ORF and UTR	SPT6 HA-Tagging	F	ACGCTTCTAAAATCTAACAGTAGTAA GAATAGAATGAACAACTACCGTcgtacg ctgcaggtcgac
			R	AGTAATAATAAAATTAATAATAACAA TGGACACTACATACGCATatcgatgaattcga gctcg
ULP2	ORF	Deleting ULP2	F	CATCACAACCAATTACATTAC
			R	AAGCAACTGTGCTGTTCATTC

Table 3: RPB1 vs rpb1-K1487R GROseq data analysis tools and parameters

Library Synthesis	NEB Ultra II Directional polyA mRNA prep
Sequencing	Novaseq SP PE 2x100bp
Quality Control	FastQC (version 0.11.9)
Genome Alignment	Program: HISAT2 v2.1.0 with sacCer3 reference genome Parameters: "- -rg PL: ILLUMINA"- -dta" "- -rna-strandedness RF"
Transcript counting	Program: subread v2.0.0; featureCounts v2.0.0; Options: "-T" "8" "-p" "-a" "-t" "exon" "-g" "gene_id" "-o"
Differential Expression analysis	edgeR (3.36.0) Parameters: Library sizes were normalized using calcNormFactors; dispersions were estimated with estimateDisp with robust argument; likelilhood ratio tests for differential expression were performed with glmFit and glmLRT

Table 4: RPB1 vs rpb1-K1487R ChIPseq data analysis tools and parameters

Library Synthesis	NEB Ultra II DNA library prep
Sequencing	Novaseq SP PE 2x100bp
Quality Control	FastQC (version 0.11.9)
Genome Alignment	Bowtie2 (version 2.3.5.1) with sacCer3 reference genome
Peak Calling	MACS (version 2.2.7.1) Parameters: paired-end; input as control; broad region calling; effective genome size 1.2e7; qvalue cutoff = 5.00e-02
Differential Binding analysis	DiffBind (3.4.9) from Bioconductor Parameters: dba.normalize (background=TRUE, normalize=DBA_NORM_NATIVE); dba.contrast (minMembers=2); dba.analyze (bGreylist=FALSE, bBlacklist=FALSE); dba.report
Peak Annotation	ChIPpeakAnno (3.28.1) from Bioconductor Parameters: TxDb.Scerevisiae.UCSC.sacCer3.sgdGene genome annotation package. annotatePeakInBatch.
Notes	GO term analysis performed as follows: Overrepresentation analysis performed at http://pantherdb.org/ Statistical overrepresentation; Fisher's Exact REGIVO dispensability cutoff: 0.5. (http://revigo.irb.hr/)